NACA

RESEARCH MEMORANDUM

LOW-SPEED CHARACTERISTICS OF A 45° SWEPT WING

WITH LEADING-EDGE INLETS

By Robert E. Dannenberg

Ames Aeronautical Laboratory
Moffett Field, Calif.

AFMDC
TECHNICAL LIBRARY

NATIONAL ADVISORY COMMITTEE
FOR AERONAUTICS
WASHINGTON
August 13, 1951

National Aeronautics and
Space Administration

NASA

Langley Research Center
Hampton, Virginia
23665

JUN 1 6 1983

Reply to Attn of   139A

TO: Distribution

FROM: 180A/Security Classification Officer

SUBJECT: Authority to Declassify NACA/NASA Documents Dated Prior to
         January 1, 1960

(informal, correspondence)

Effective this date, all material classified by this Center prior to
January 1, 1960, is declassified. This action does not include material
derivatively classified at the Center upon instructions from other Agencies.

Immediate re-marking is not required; however, until material is re-marked by
lining through the classification and annotating with the following statement,
it must continue to be protected as if classified:

     "Declassified by authority of LaRC Security Classification Officer (SCO)
     letter dated June 16, 1983," and the signature of person performing the
     re-marking.

If re-marking a large amount of material is desirable, but unduly burdensome,
custodians may follow the instructions contained in NHB 1640.4, subpart F,
section 1203.604, paragraph (h).

This declassification action complements earlier actions by the National
Archives and Records Service (NARS) and by the NASA Security Classification
Officer (SCO). In Declassification Review Program 807008, NARS declassified
the Center's "Research Authorization" files, which contain reports, Research
Authorizations, correspondence, photographs, and other documentation.
Earlier, in a 1971 letter, the NASA SCO declassified all NACA/NASA formal
series documents with the exception of the following reports, which must
remain classified:

Document No.	First Author
E-51A30	Nagey
E-53G20	Francisco
E-53G21	Johnson
E-53K18	Spooner
SL-54J21a	Westphal
E-55C16	Fox
E-56H23a	Himmel

JUN 2 3 1983

NATIONAL ADVISORY COMMITTEE FOR AERONAUTICS

RESEARCH MEMORANDUM

LOW–SPEED CHARACTERISTICS OF A 45° SWEPT WING

WITH LEADING–EDGE INLETS

By Robert E. Dannenberg

SUMMARY

An investigation was conducted to determine the low–speed aerodynamic characteristics of a 45° swept wing with leading-edge inlets. The wing had a constant chord and completely spanned the wind tunnel. The inlets extended over approximately the central third of the span of the wing and the height of the entrance was varied from 15 to 50 percent of the maximum thickness of the wing. Pressure–distribution and wake–survey measurements were obtained for the wing with various inlet shapes.

The wing with an inlet was found to possess section characteristics which were, in general, similar to those of the comparable plain swept wing for only a small range of positive angles of attack. Within this range, the losses of ram pressure within the inlets were small. At some positive angle of attack a region of separated flow developed on the upper surface of the ducted section of the wing near the leading edge. With flow separation, the lift generally was increased over the span of the inlet and was decreased over the span of the wing downstream of the inlet.

INTRODUCTION

The information available in regard to the proper shape for an air inlet opening on a swept wing is meager; the data that are available consist of the results of tests to develop air inlets for specific uses. One study, described in reference 1, consisted of tests of various shape openings on a wing with the leading–edge line swept 40°. These tests were made only for an angle of attack of 0°. Other applications were designed for ram–jet installations in which the inlets extended along the full span of the wings (references 2 and 3).

An investigation of a method, employing a lofting technique, for the design of leading-edge inlets in unswept wings was reported in reference 4. A wing with inlets designed by this method was found to possess satisfactory lift, drag, and pressure-distribution characteristics.

This report presents the results of an investigation of the effects accompanying the addition of various leading-edge inlets to a wing set obliquely to the free-stream direction. Several of the inlet profiles tested were geometrically similar to those tested on the unswept wing as reported in reference 4.

In order to make the present investigation comparable with that of reference 4 the leading-edge inlets were fitted to a constant-chord wing having the same section normal to the leading edge, but with the leading edge swept 45°. The swept wing was mounted across one of the Ames 7- by 10-foot wind tunnels as the experimental results in reference 5 had indicated that the flow over the central portion of the span of the plain swept wing satisfactorily approximated the flow about a yawed wing of infinite span as given by simple sweep theory.

SYMBOLS AND COEFFICIENTS

The symbols which indicate the geometric properties of the plain and ducted airfoil sections are shown in figure 1. All geometric dimensions are in percent of the chord. Force and moment coefficients are based on the chord in the stream direction.

a   distance from origin of upper-lip leading-edge radius to chord line

A   entrance area, corresponding to span of the inlet times the inlet-entrance height (d), square feet

b   distance from origin of lower-lip leading-edge radius to chord line

c_d external wake drag coefficient

c_l section lift coefficient

c_m section pitching-moment coefficient about the quarter-chord point

d   inlet-entrance height

H   total pressure, pounds per square foot

ΔH decrement in total pressure, pounds per square foot

$\dfrac{H_1 - p_0}{H_0 - p_0}$ ram-recovery ratio

k_1, k_2 interference factors

p static pressure, pounds per square foot

P pressure coefficient $\left(\dfrac{p_l - p_0}{q_0} \right)$

q dynamic pressure, pounds per square foot

r lip radius

t maximum thickness of airfoil section

V velocity, feet per second

$\dfrac{V_1}{V_0}$ inlet-velocity ratio

x distance along chord measured perpendicularly from leading edge

y ordinate of section measured perpendicularly from the chord line

α angle of attack in streamwise plane, degrees

φ stagger of inlet opening measured in a plane perpendicular to the leading edge, (acute angle between line normal to chord line and line joining the origins of the upper- and lower-lip radii), degrees

Subscripts

o free-stream

l local

u uncorrected

1   in duct inlet at rake station (5 percent of the chord
              behind the leading edge)

MODEL AND APPARATUS

A sketch of the model installation and of a typical section
through the central portion of the model are shown in figure 1.

The model was a constant-chord wing swept 45° and extended from
side wall to side wall of the wind tunnel as shown in figure 2.
Sections perpendicular to the leading edge of the plain wing were the
NACA 63_1-012 with a chord of 2.5 feet. Coordinates for the NACA 63_1-012
section are given in reference 6. The axis of rotation for angle-of-
attack changes was perpendicular to the stream direction and crossed the
chord line of the midspan station of the wing at 35 percent of the
chord. A removable inlet occupied the central portion of the span.

The leading-edge inlets investigated on the wing are illustrated
in table I and the coordinates of the lips are tabulated in table II.
The entrance heights varied from 0.15 to 0.50 of the maximum thickness
of the airfoil. The profiles shown in table I are those perpendicular
to the leading edge of the wing. The shape of the airfoil behind its
maximum thickness remained unchanged. The inlet profiles and the means
of fairing the inlets into the solid wing in the spanwise direction
were determined, with some modification, according to the design method
discussed in reference 4. No attempt was made to simulate an aircraft
internal-duct system insofar as the inner-surface coordinates were con-
cerned.

Air was drawn through the inlets into the hollow spar in the wing
and then through a ducting system by a compressor outside the test
chamber. The quantity of air flowing through each inlet was calculated
from the pressure drop across a calibrated orifice plate. For the
large inlets, the maximum value of inlet velocity was limited by the
output of the compressor so that in order to obtain an inlet-velocity
ratio of 0.8, the spanwise length of the higher openings was reduced
from 40 percent of the span to 24 percent of the span. The entrance
areas in the inlets are given in the following table:

d/t	0.15	0.20	0.25	0.35	0.50
A (sq ft)	.18	.24	.30	.25	.36

Bench tests of a model simulating the internal duct system
(fig. 3) indicated that the inlet velocity would not be uniform across
the span of the opening unless guide vanes were used within the duct to

proportion the flow properly. The vane arrangement that provided the best distribution of flow at the inlet and that which was used for the wind-tunnel tests is shown in figure 3. A screen was also placed at the entrance to the spar (fig. 1(b)) to improve further the entrance flow distribution.

The pressure distributions over the upper and lower surfaces of the wing were determined by means of flush orifices distributed over the surface of the model as indicated in figure 4. The pressure distributions over the inner surfaces of the inlet lips were measured at the midspan by flush orifices 0.5, 1.25, and 2.5 percent of the chord from the leading edges of the upper and lower lips.

The inlet pressure losses were measured by means of rakes of total-pressure tubes 5 percent of the chord behind the leading edge. These rakes were located at various spanwise stations along the inlet. The rake tubes were parallel to the chord plane, were alined in the direction of the free stream, and were equally spaced as noted in figure 1(b). The arithmetic mean of the pressures indicated by the individual rake tubes was used to calculate the ram-recovery ratio.

The lateral deviations of the flow direction in the inlets relative to the free stream were measured by means of small prong-type directional pressure rakes. (See fig. 5(a).) The rakes were located near the midspan of the various inlets (52-percent-span station). For one inlet (d/t of 0.25 with 20° stagger), directional rakes were also located on both sides of the midspan of the inlet (38 and 60 percent of the wing span).

The wake pressures used in calculation of the wake drag were measured by a survey rake that was connected to an integrating manometer. The tubes of the rake were in a plane perpendicular to the chord plane and were alined in the direction of the free stream. The traverse of the survey rake behind the wing is indicated in figure 4.

TESTS

The swept wing with the various inlets illustrated in table I was tested at angles of attack from 0° to 12°. Whenever possible, the tests were made with a free-stream dynamic pressure of 40 pounds per square foot, which corresponded to a Mach number of 0.16. The Reynolds number for this dynamic pressure was 3,900,000 based on the chord in the stream direction. In some cases, however, in order to obtain higher values of inlet-velocity ratio, the dynamic pressure was reduced to 30 pounds per square foot which corresponded to a Reynolds number of 3,400,000. The wake-drag measurements were made at a dynamic pressure corresponding to a Reynolds number of 6,200,000.

The section lift and section pitching-moment coefficients for the wing were obtained by integration of the chordwise pressure-distribution curves. The tunnel-wall correction to the angle of attack, applied according to the methods discussed in reference 5, is given by the following equation:

$$\alpha = \alpha_u + \frac{k_1 \, c_l}{1 + k_2 c_l}$$

The values of k_1 and k_2 along the span of the wing (from reference 5) are given in figure 6(a) and the variation of the correction along the span is given in figure 6(b) as a function of section lift coefficient.

The wake drag coefficients were calculated from the distributions of static pressure and total-pressure loss through the wake by the methods discussed in reference 7.

With the guide vanes in the internal duct as shown in figure 3(b) and a screen at the spar entrance as shown in figure 1(b), the velocity at all points in the inlet was within 3 percent of the mean inlet velocity.

As the rake tubes used to measure the inlet pressure losses were alined in the direction of the free stream, it was necessary to evaluate the effect of the angularity of the flow on the pressures as indicated by the total-pressure tubes. The total-pressure error of the rake tubes due to changes in the flow direction shown in figure 5(c) was determined from the results presented in reference 8. When the change of the lateral flow angle with the inlet-velocity ratio was considered, it was noted that the largest observed error of ram-recovery ratio was less than 0.03. Since the correction factors for flow angularity would be very small, at least at the center of the inlet, the measurements of ram-recovery ratio were not corrected for the flow angularity.

RESULTS AND DISCUSSION

Surface-Pressure Characteristics

Chordwise distribution at midspan.- The chordwise variations of the pressure coefficients over the external surfaces of several of the ducted airfoil sections are presented in figures 7, 8, and 9 for an inlet-velocity ratio of 0.8. For small positive angles of attack the pressure distributions are of the shape indicated by the solid line in

the sketch. The type of flow asso-
ciated with this pressure distribu-
tion is termed "attached flow." At
some positive angle of attack, a par-
tial collapse of the pressure peaks
over the leading edge of the upper
surfaces occurred, accompanied by the
formation of a region of approximately
constant pressure as indicated by the
dashed line in the sketch. This latter
type of flow is termed "separated flow."
A summary of the data showing the angles
of attack at which the external flow
separated for the inlets illustrated in
table I(a) is given in figure 10. A study of the pressure distribution
over the plain wing as reported in reference 5 did not indicate any com-
parable separation for angles of attack from 0° to 12°.
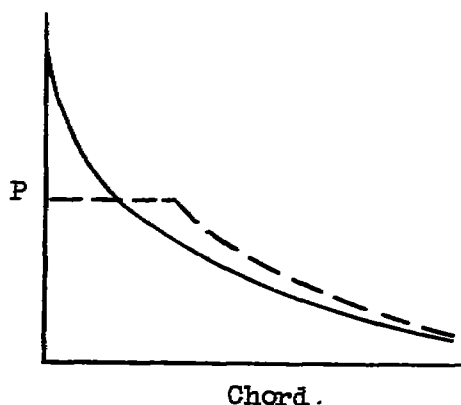
It is of interest to note that the inlets with stagger encountered
flow separation at smaller angles of attack than did those without
stagger. The lip radius and thickness distribution of the upper lip of
an inlet having a d/t of 0.20 with 20° stagger were varied as illus-
trated in table I(b). The results are given in figure 11. The
increased thickness of the upper lip with constant lip radius raised the
angles of attack at which separation was first indicated to values
nearly equal to those for the unstaggered inlets.

With attached flow over the inlets, the pressure coefficients on
the forward 15 to 25 percent of the airfoil differed from those over the
plain airfoil (reference 5) in a manner depending on the inlet-velocity
ratio. Typical pressure distributions for inlet-velocity ratios of
0, 0.4, and 1.2 are presented in figure 12(a) for an inlet with a d/t
of 0.25 and 20° stagger. The distribution for an inlet-velocity ratio
of 0.8 is given in figure 7(b). Values of the minimum pressure coeffi-
cient on the upper surfaces of the various inlets for the inlet-
velocity ratios obtained in the present test are given in table III.

For positive angles of attack, the change in the pressure distribu-
tions over the lower external surfaces due to inlet-velocity ratio was
small and for most engineering purposes the pressure distribution could
be considered unchanged from that presented for an inlet-velocity ratio
of 0.8.

Comparison at equal angles of attack of the pressure distributions
for the inlets with attached flow with those for the plain airfoil
between approximately 20-percent chord and 60-percent chord revealed
that, in this region, the pressure coefficients behind the inlets were
less negative than those for the plain airfoil for all test values of

inlet—velocity ratio. From approximately 60—percent chord to the trailing edge, the pressure distributions remained essentially unchanged from those of the plain airfoil.

The pressures over the inner surfaces of the inlet lips were measured by orifices 0.5, 1.25, and 2.5 percent of the chord from the leading edges of the upper and lower lips. At zero angle of attack the measured pressures on the inner surfaces of the upper and lower lips were essentially of the same value. For positive angles of attack, the minimum pressure occurred at 0.5—percent chord on the lower lip with slightly increased pressures at the two downstream orifices on the lower lip and over the inner surface of the upper lip. The minimum pressure coefficients on the inside surfaces of the lower lips are given in figure 13 for angles of attack of 0°, 4°, and 8°.

Spanwise distribution.— The addition of an inlet on the swept wing resulted in a change in the spanwise distributions of pressure compared to those for the plain wing as given in reference 5. The pressure distributions over the wing adjacent to the ducted portions of the wing (i.e., the 27.5— and 72.5—percent—span stations) as well as the spanwise distributions along the 5—, 15—, 30—, 50—, and 80—percent—chord lines, shown in figures 14 to 16, are representative of those for the model with the inlets tested in this investigation.

With attached flow over the inlet section, the spanwise distribution was relatively unchanged from the distribution for the plain wing. However, with the onset of separation, the section load distribution over the ducted wing underwent an abrupt change. The load distribution over the portion of the wing, the leading edge of which was upstream of the inlet, was effectively unchanged. Over the ducted portion of the wing the changes in distribution with inlet shape were commensurate with the data shown in figures 7 to 12. In addition, the magnitude and the spanwise portion of the minimum pressure coefficient changed with angle of attack, as exemplified by figures 15(a) and 15(b).

Comparison with results predicted from tests of unswept inlet.— Simple sweep considerations indicate that pressure coefficients for a swept wing of infinite aspect ratio should vary as the square of the cosine of the angle of sweep. This was shown to be the case experimentally in reference 5 for a region over the central half of the span of the wing without an inlet. In figure 12(b), the measured pressure distributions over the upper surface of the swept wing having an inlet with a d/t of 0.25 and 20° stagger and the distribution computed from the results for a similar inlet on the unswept wing are compared at two angles of attack. The corresponding angle of attack of the unswept wing was determined from the relation

$$\alpha_{swept \ wing} = \alpha_{unswept \ wing} \times \cos 45°$$

As noted in figure 12(b), the agreement of the computed pressure
coefficients with the measured pressure coefficients was good for an
angle of attack of 0° except for an inlet-velocity ratio of zero ahead
of about 6-percent chord. For an angle of attack of 4.14°, the agree-
ment of the computed values with the measured values behind about
20-percent chord was also good; however, nearer the leading edge the
measured pressure coefficients were somewhat less negative than those
predicted by the cosine-squared relationship of simple sweep theory.
Within this region near the leading edge the predicted effect of inlet-
velocity ratio was approximately correct, but it appears that the effect
of angle of attack on the pressure distributions was not adequately
taken into account by simple sweep considerations.

The results of tests of inlets on the unswept wing reported in
reference 4 indicated that increasing the inlet-velocity ratio
increased the maximum lift coefficient until values equal to that of the
plain airfoil were obtained. Re-examination of these data indicated
that flow separation near the leading edge occurred at an angle of
attack slightly lower than that at which the plain wing stalled. For
the unswept wing with an inlet having a d/t of 0.15 and 20° stagger,
separation occurred for angles of attack between 9° and 10° for an
inlet-velocity ratio of 0.4 and between 11° and 12° for an inlet-
velocity ratio of 0.8. For the similar inlet on the swept wing, the
angles of attack at which separation occurred were 6.7° and 7.5° for
inlet-velocity ratios of 0.4 and 0.8, respectively. (See figure 10(a).)
These data would indicate that the corresponding angles of attack for
flow separation are given approximately by the cosine relation.

In reference 4, a method is presented whereby the effects of
changes in inlet ordinates, camber, inlet-velocity ratio, and angle of
attack on the velocity distribution for an inlet on an unswept wing can
be calculated. (See equation (13) of reference 4.) The local veloci-
ties are broken down into various components as is done in the case of
airfoils in potential flow (reference 6). To determine whether this
method could be adapted to inlets on a swept wing, calculations were
made of the velocity distributions over lips 21 and 23 (table I(b)) for
inlet-velocity ratios of 0, 0.8, and 1.6 using the coordinates and data
for lip 9 as a base. The numerical procedure employed was similar to
that discussed in the appendix of reference 4.

Computations made for angles of attack with attached flow over the
inlets agreed well with the experimental results when the experimental
velocity distributions from lip 9 were used as the basic distribution.
Attempts to predict the velocity distribution over lips 21 and 23 using
the experimental data from the unswept counterpart of lip 9 adjusted
for the effects of sweep did not provide completely satisfactory agree-
ment.

Lift and Pitching–Moment Characteristics

The lift characteristics for a section at the midspan of the wing
with various leading–edge inlets are shown in figure 17. Similar data
for the plain swept wing (obtained from reference 5) are also shown
for comparison. The lift coefficients were obtained by integration of
the chordwise pressure–distribution diagrams. Typical lift curves for
sections on each side of the ducted portion of the wing (the 27.5– and
72.5–percent–span stations) are shown in figure 18, while the pitching–
moment characteristics at the three stations are given in figure 19.

The variations of section lift coefficient along the span of the
plain wing without an inlet are presented in reference 5. The ref-
erence results indicated that the section lift coefficients were rela-
tively constant between the 27.5– and 72.5–percent–span stations for
given corrected angles of attack. At a corrected angle of attack of 10°
the section lift coefficient at 27.5–percent span was 0.71 and increased
linearly to 0.75 at 72.5–percent span. The results of the present
investigation indicate that adding an inlet to the wing had but a small
effect on the spanwise variation of lift for angles of attack from 0°
to 6° or 8°. For higher angles of attack, the lift–curve slope
decreased for sections of the wing downstream of the inlet and at
72.5–percent span the lift was below that of the plain wing as indi-
cated in figure 18. Increasing inlet–velocity ratio resulted in
increased lift over this portion of the wing and reduced lift over the
ducted section of the wing.

There was no perceptible change in the pitching–moment character-
istics about the one–quarter-chord point of a section of the wing with
an inlet compared to that of the plain swept wing.

Wake–Drag Characteristics

Associated with the onset of flow separation over the upper
surface of the ducted portion of the wing there was an abrupt change in
the drag characteristics as computed from wake–survey measurements.
The change in drag was characterized by changes in the size and shape of
the wake. For positive angles of attack less than those for which sepa-
ration occurred, the total pressure through the wake varied in a manner
similar to a cosine–squared curve. When flow separation occurred, the
wake width increased and the maximum pressure loss decreased, although
the integrated pressure loss, and hence the drag, increased. The span-
wise variations of the wake drag coefficients for four wing–inlet com-
binations are shown in figures 20 through 23. With attached flow, the
wake drags decreased with increasing inlet–velocity ratio.

The increase in wake drag of the entire wing panel due to the
addition of an inlet was obtained by integrating over the span of the
survey the increment in local wake drag due to the inlet. For an
inlet-velocity ratio of 0.8, the addition of the inlet noted in
figure 20 resulted in a computed increment of drag coefficient based on
the wing area of 0.0001 and 0.0003 for uncorrected angles of attack of
0° and 5°, respectively. With zero inlet-velocity ratio and for 0°
angle of attack the increment was 0.0010. From inspection of figures 21
to 23 it is apparent that the drag increment increased slightly as the
inlet height was increased.

Internal-Flow Characteristics

The local ram-recovery ratios for three inlets having d/t ratios
of 0.20, 0.35, and 0.50 with the lips staggered 20° are shown as
functions of the angle of attack in figure 24. The angle-of-attack
range for high ram-recovery ratio was small. The reduction in the ram-
recovery ratio for the higher angles of attack apparently was due to
flow separation from the inner surface of the lower lip.

Tests with several inlets indicated that the direction of the flow
at the inlet was approximately parallel to the leading edge of the wing
at zero inlet-velocity ratio. As the inlet-velocity ratio increased up
to 1.2, the flow direction approached that of the free stream as shown
in figure 5(b). The shaded area in figure 5(b) represents the range of
flow angles obtained for positive angles of attack with attached flow
over the inner surface of the lower lips. No systematic variation in
the flow direction with inlet geometry was noted.

CONCLUDING REMARKS

The results of an investigation of inlets installed in the leading
edge of a 45° swept wing having the NACA 63_1-012 section perpendicular
to the leading edge indicated the following:

At some positive angle of attack, the flow over the ducted portion
of the wing was characterized by the pressure peak over the leading
edge of the upper lip being replaced by a region of approximately con-
stant pressure. As the angle of attack was increased, the constant-
pressure region extended over a larger portion of the chord. This flow
separation was delayed to higher angles of attack by decreasing the
entrance-height ratio, by increasing the thickness at the nose of the
upper lip, or by decreasing the stagger.

The differences in the spanwise variation of lift characteristics, as for the plain wing, were found to be small for positive angles of attack up to 6° or 8°. At higher angles of attack the flow separated, and the lift generally was increased over the ducted portion of the wing and was decreased over the portion of the wing downstream of the inlet.

The spanwise variations in the wake-drag and moment characteristics of the inlet section with internal air flow were, in general, small except where affected by the flow separation.

The angle-of-attack range for high ram-recovery ratio was small. Flow separation from the inner surfaces of the lower lips apparently caused a reduction in ram-recovery ratio for the higher angles of attack.

Ames Aeronautical Laboratory,
    National Advisory Committee for Aeronautics,
        Moffett Field, Calif.

REFERENCES

1. Scherrer, A.: Investigation of Air Inlets at the Leading Edge of Sweptback Wings. Zentrale für Wissenschafttiches Berichtswesen der Luftfahrtforschung, Berlin, UM 3188, Nov. 24, 1944.

2. Douglass, William M.: Wing-Ramjet Development. Summary Report. USCAL Report 3-9, June 15, 1948.

3. Küchemann, D., and Weber, J.: Two Dimensional Intake Contours. AVA Monographs, A. Betz, ed., J_2 Power Unit Ducts. Ministry of Aircraft Production, Rep. and Trans. No. 987, June 1, 1948.

4. Dannenberg, Robert E.: A Design Study of Leading-Edge Inlets for Unswept Wings. NACA RM A9K02b, 1950.

5. Dannenberg, Robert E.: Measurements of Section Characteristics for a 45° Swept Wing Spanning a Rectangular Low-Speed Wind Tunnel as Affected by the Tunnel Walls. NACA TN 2160, 1950.

6. Abbott, Ira H., Von Doenhoff, Albert H., and Stivers, Louis S., Jr.: Summary of Airfoil Data. NACA Rep. 824, 1945. (Formerly NACA ACR L5C05, 1945)

7. Heaslet, Max A.: Theoretical Investigation of Methods for Computing
        Drag from Wake Surveys at High Subsonic Speeds. NACA ARR
        5C21, 1945.

8. Humphreys, Milton D.: Effects of Compressibility and Large Angles
        of Yaw on Pressure Indicated by a Total-Pressure Tube. NACA
        RB L5C30, 1945.
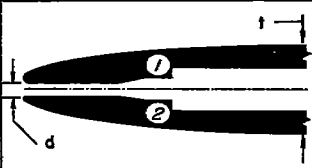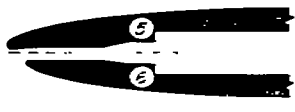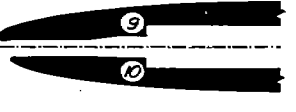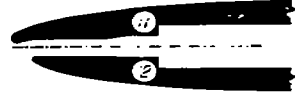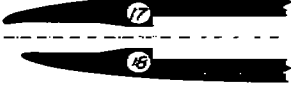
TABLE I

LEADING-EDGE INLETS TESTED

(a) Inlets designed according to the method discussed in reference 4.

d/t	Stagger		
	0°	20°	35°
0.15	1, 2	3, 4	5, 6
.20	7, 8	9, 10	11, 12
.25		13, 14	15, 16
.35		17, 18	
.50		19, 20	

TABLE I - CONCLUDED

(b)   Modifications   to   inlet   shape 9-10
(d/t ,   0.20   with   20°   stagger).
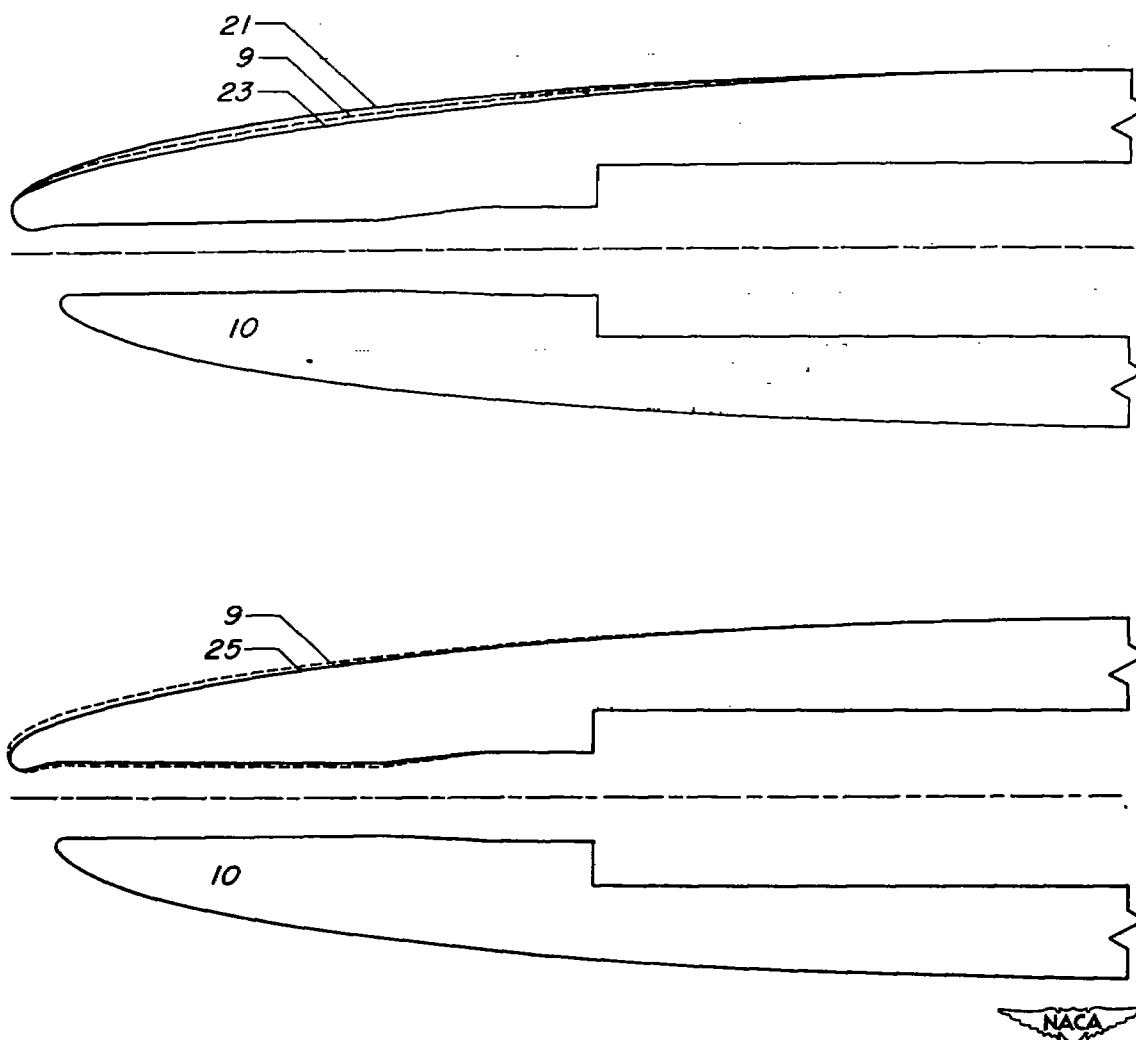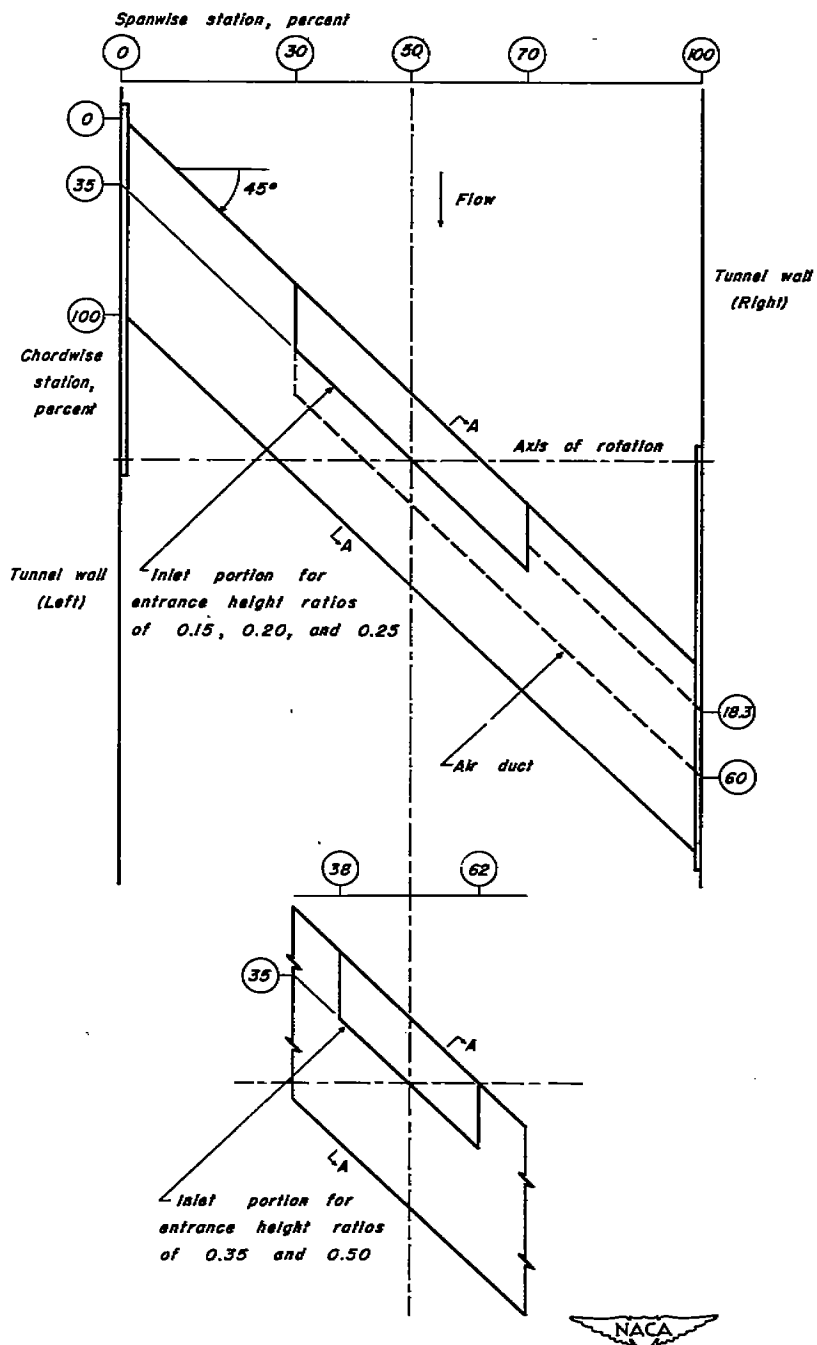
(a) Plan form of model wing showing removable portions.

Figure 1.— Arrangement of wing-inlet combination.

Chordwise station, percent

0   5   11,7   15   35   63.3   100

Inlet section   NACA 63, - 012

5.83

3

Chord line

a

b

t

φ

d

12-mesh screen
(wire diam., 0.025 in.)

Vanes not shown

All dimensions in percent
of the chord unless
otherwise noted.

Rake
(Tube spacing, 0.15 in.)

NACA
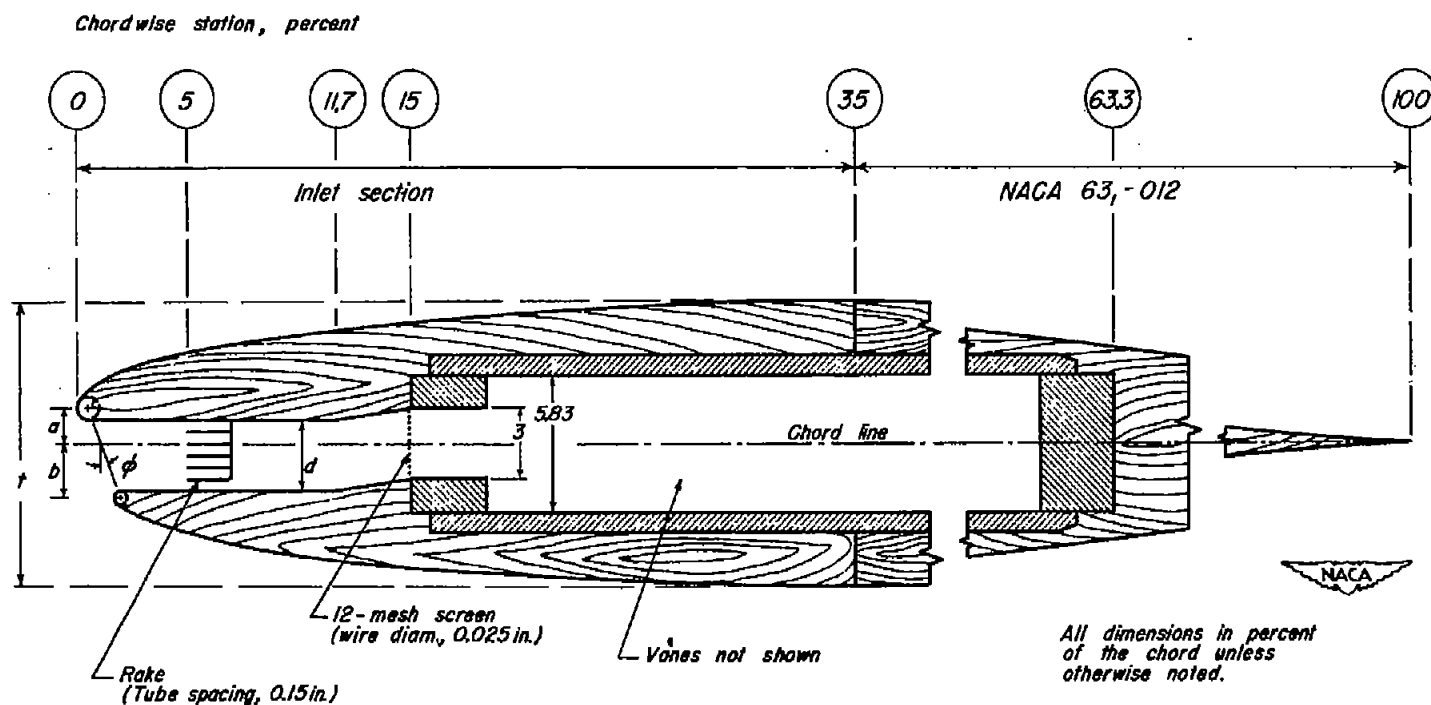
(b) Section A-A.

Figure I.- Concluded.
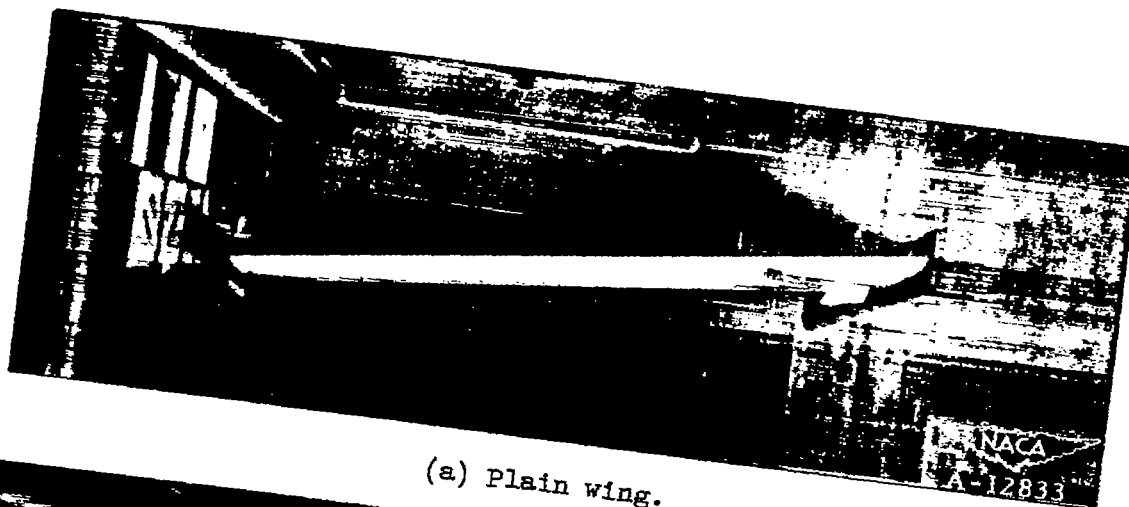
(a) Plain wing.
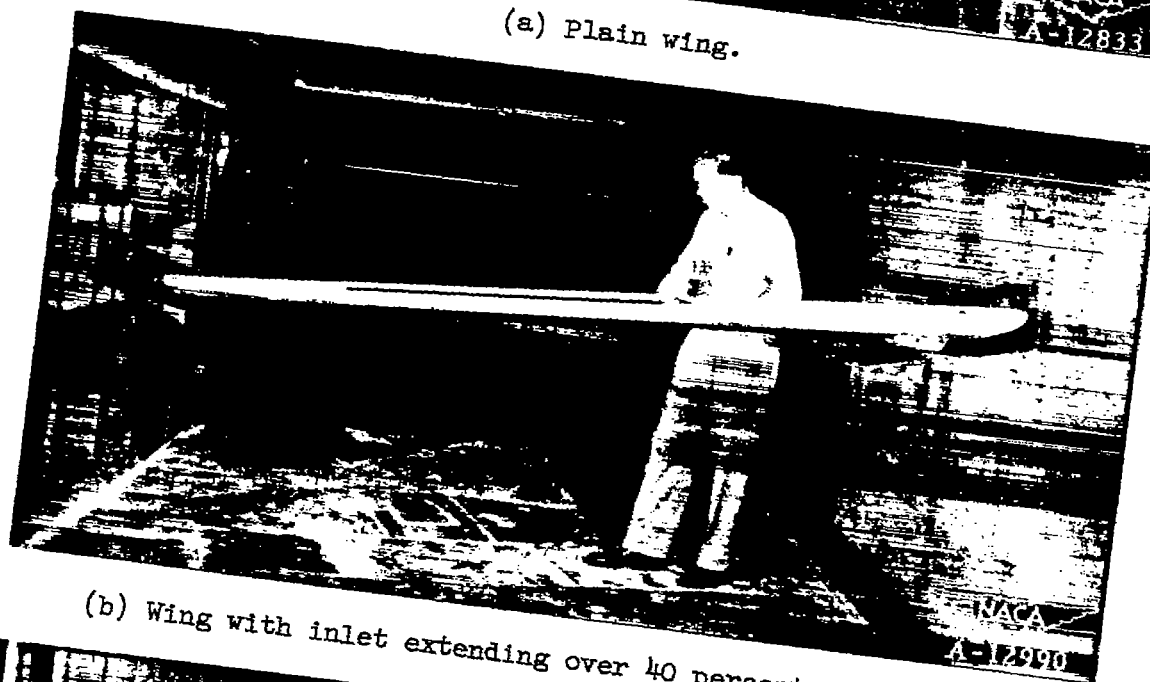
(b) Wing with inlet extending over 40 percent of the span.
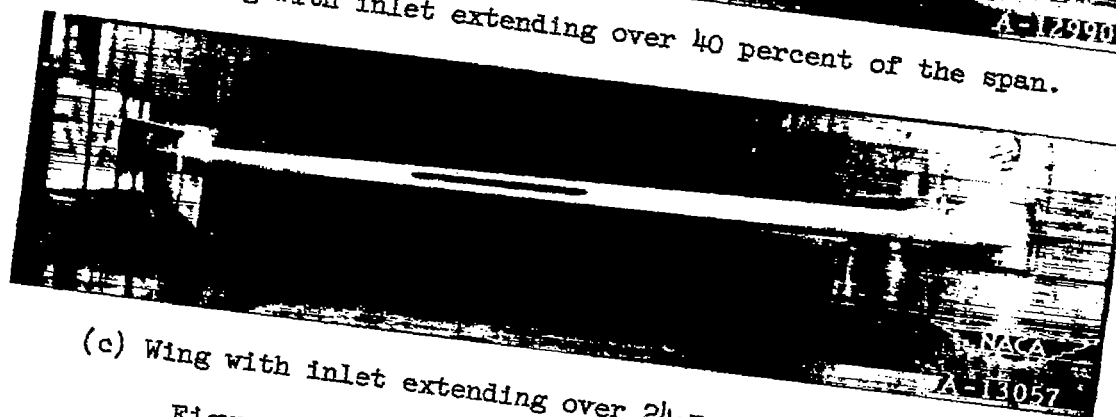
(c) Wing with inlet extending over 24-percent of the span.

Figure 2.- Model installation in wind tunnel.
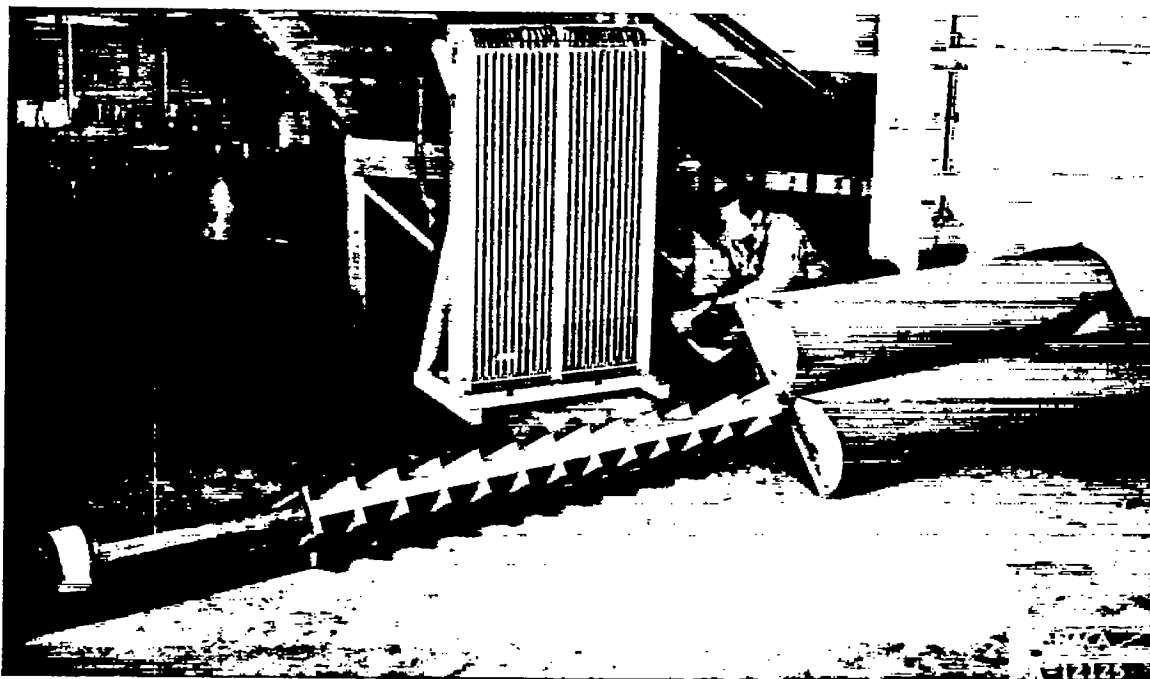
(a) General view showing bell-mouth entrance.
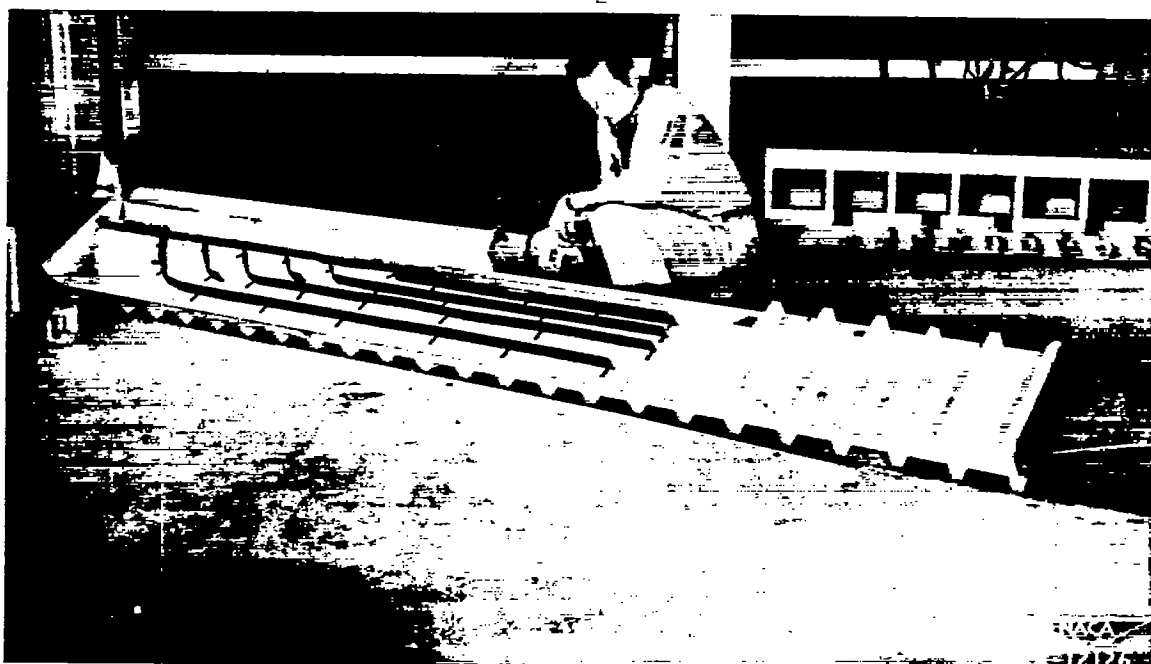
(b) Vane arrangement.

Figure 3.- Bench-test model.

Spanwise station, percent

⓪   ㉗㋝   ㊿   ⑦㋛   ⑩⓪

⑤
⑮
㉚
㊿
⑧⓪

Flow

Tunnel wall
(Right)

Chordwise
station,
percent

Axis of rotation

Tunnel wall
(Left)

Pressure
orifices

Wake-survey
location
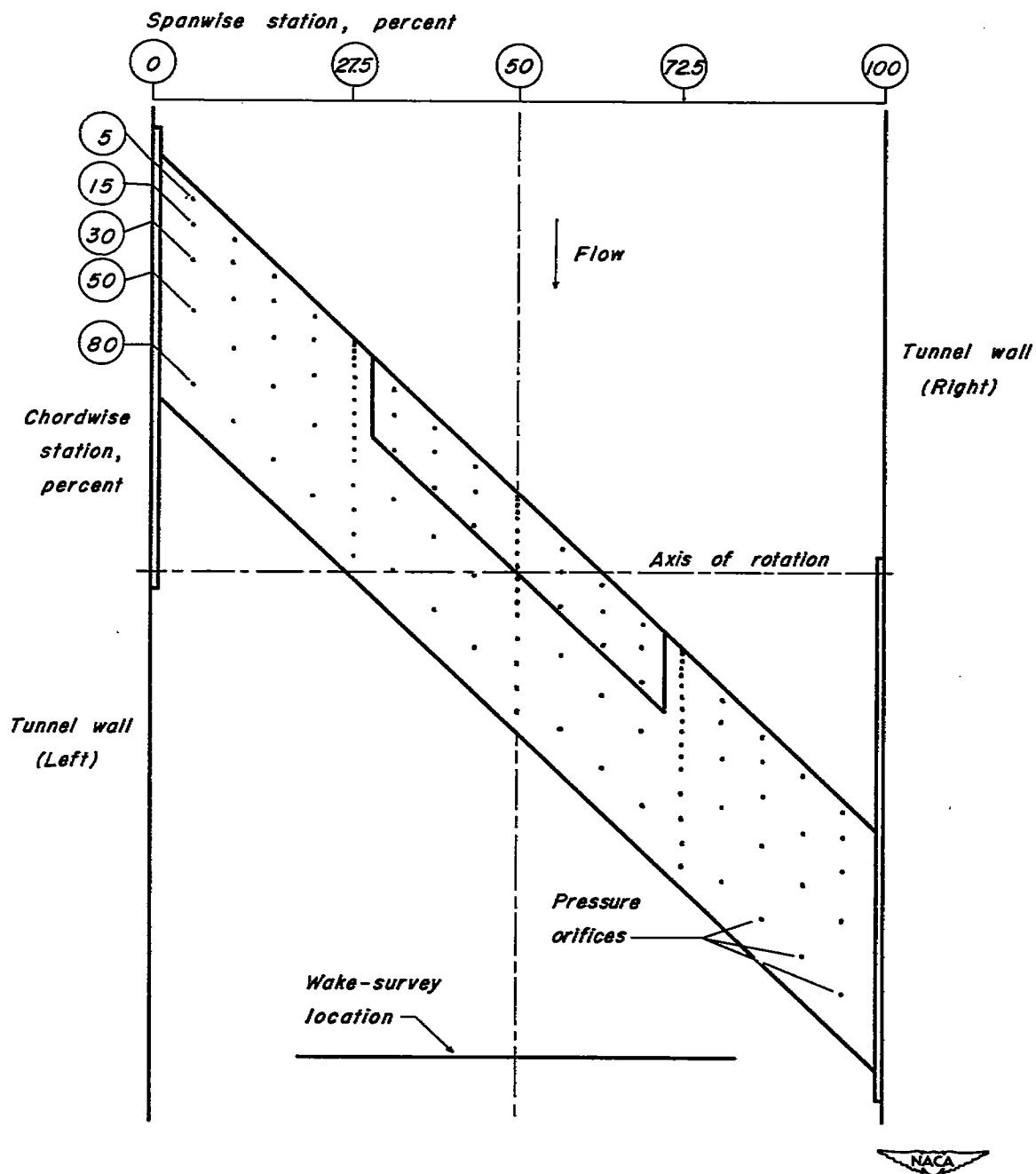
Figure 4.— Schematic diagram of the arrangement of pressure orifices
and location of the wake-survey plane.

(a)   Prong—type   directional   rake.
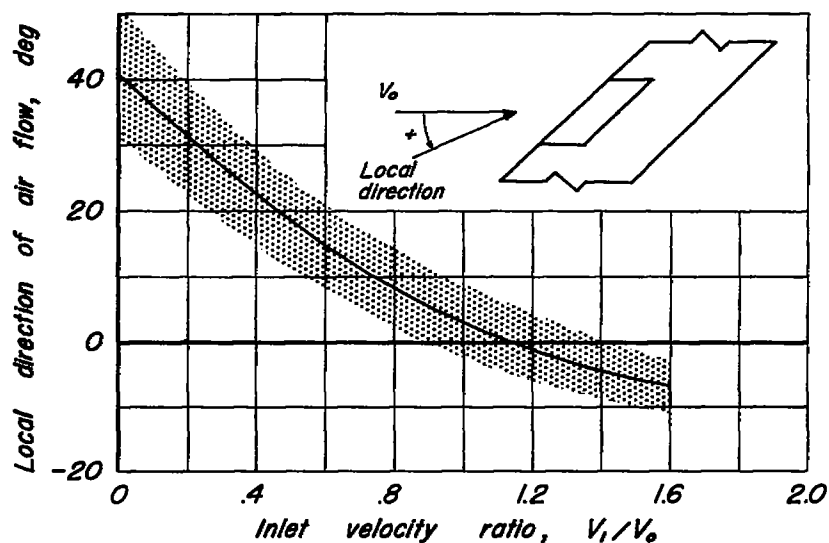
(b)   Direction   of   air   flow   in   inlet   at   5-percent
chord   of   midspan   station.
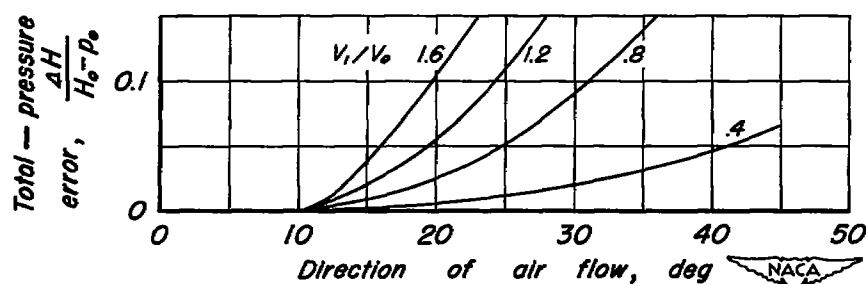
(c)   Variation   of   total-pressure   error   with   local
direction   of   air   flow   for   a   total-pressure
tube.

Figure   5.- Direction   of   air   flow   and   its   effect   on   total-pressure
error   in   the   inlets.
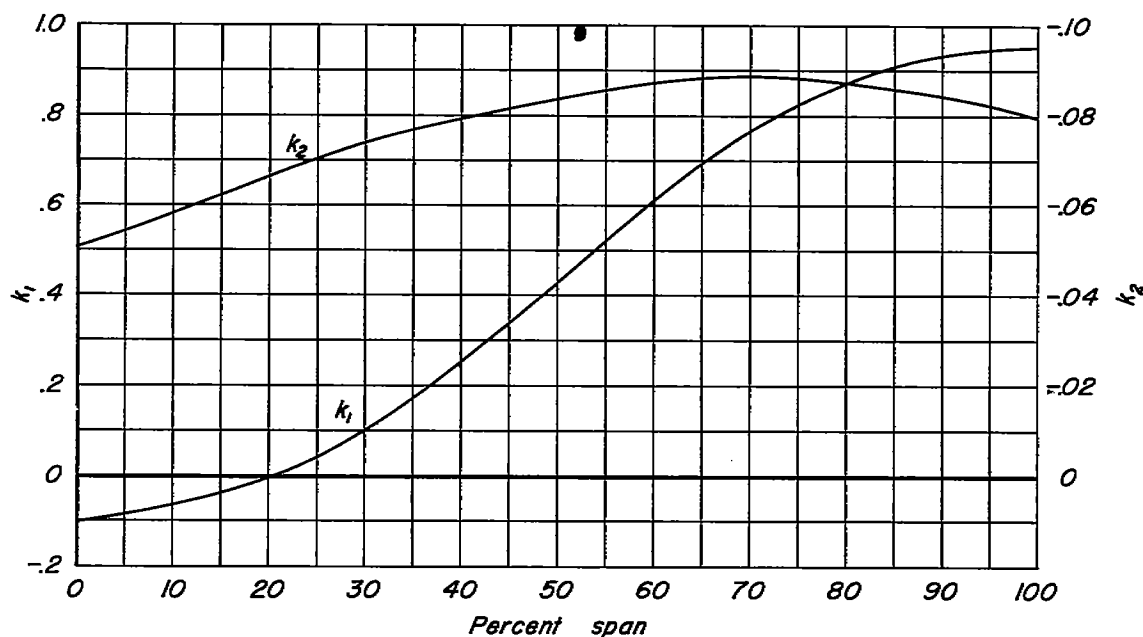
(a) Variation of factors k_1 and k_2 along the span of the wing (from reference 5).

$$\alpha = \alpha_u + \frac{k_1 c_l}{1 + k_2 c_l}$$
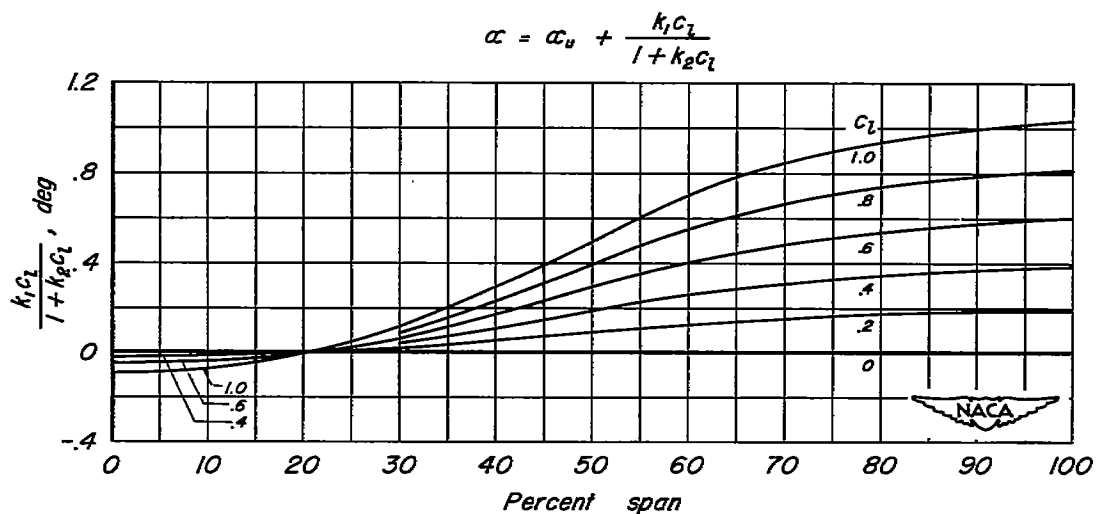
(b) Variation of the correction to the angle of attack with section lift coefficient along the span of the wing.

Figure 6.- Tunnel-wall correction for induced upwash velocity for the 45° swept wing mounted horizontally in an Ames 7- by 10-foot wind tunnel.

(a) d/t, 0.15.

(b) d/t, 0.25.
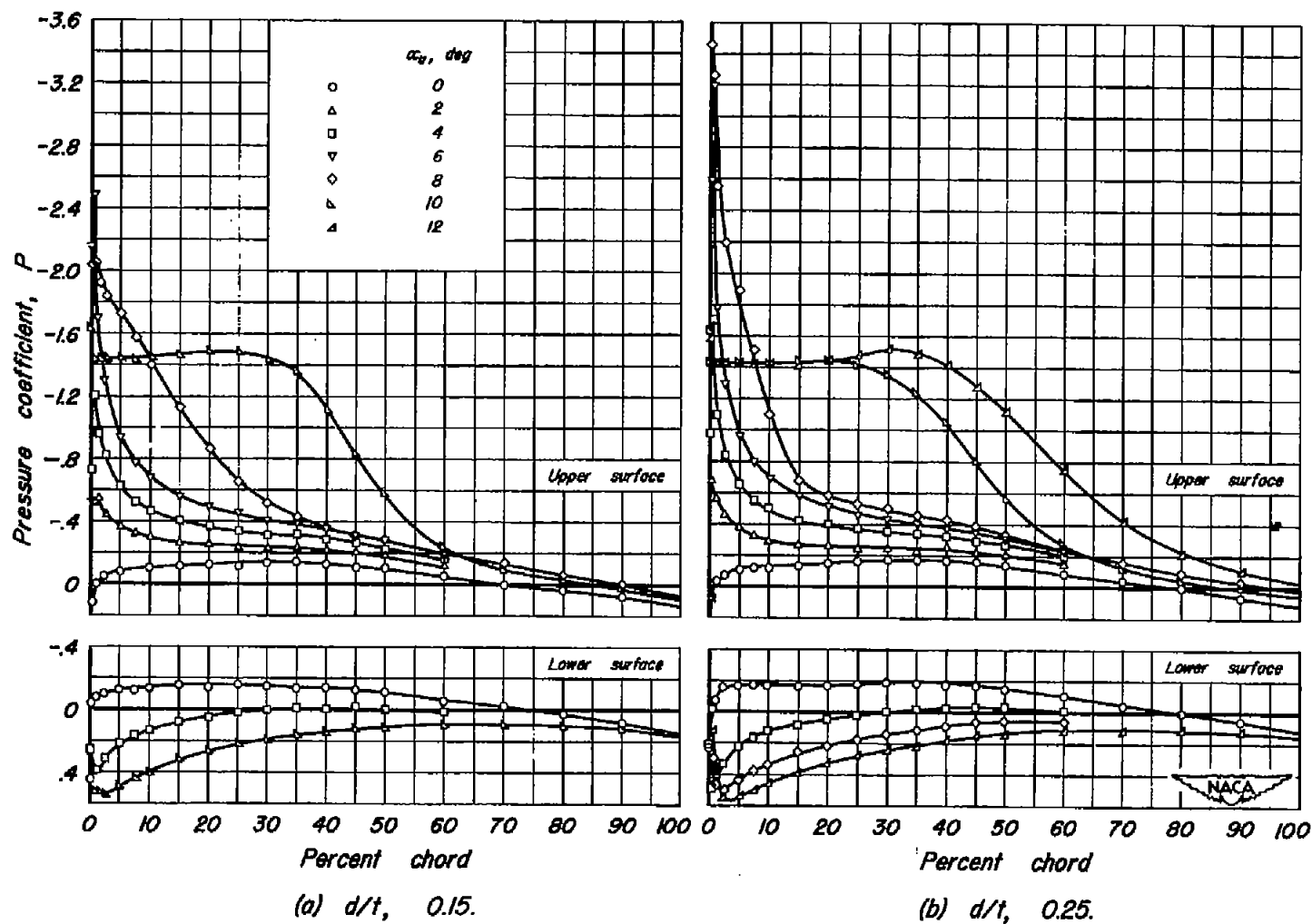
Figure 7.- Chordwise distribution of pressure at the midspan of inlets with various entrance-height ratios and 20° stagger. V_i/V_o, 0.8.

α_u, deg

○	0
△	2
□	4
▽	6
◇	8
▲	10
▲	12

Upper surface

Lower surface

Percent chord

(c) d/t, 0.35.

Upper surface

Lower surface

Percent chord

(d) d/t, 0.50.
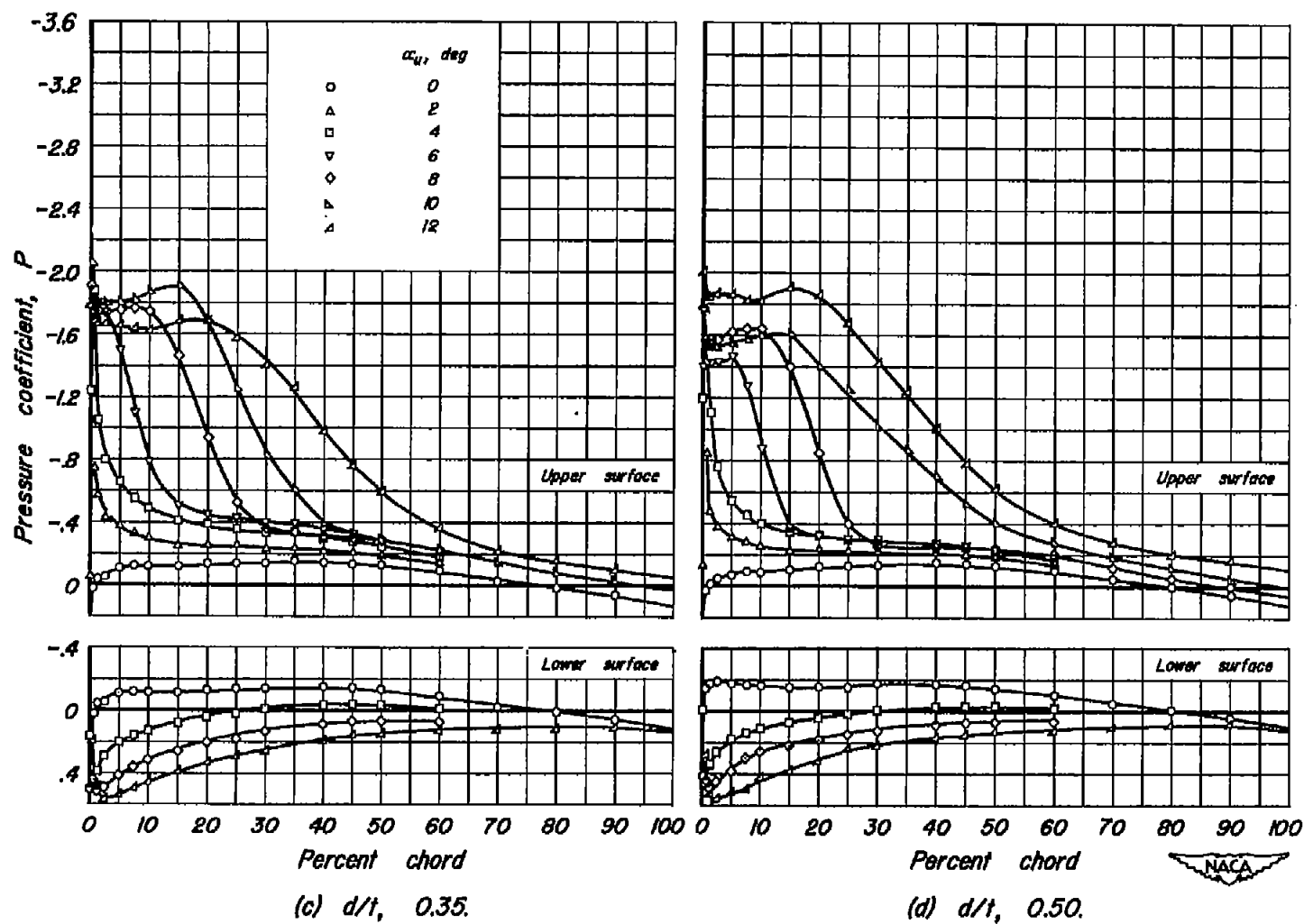
Figure 7.— Concluded.

Figure 8.— Chordwise distribution of pressure at the midspan of an inlet having a d/t of 0.20 without stagger and with 35° stagger. V_l/V_o, 0.8.

(a) Lip 9 (radius = 0.00576 c).

(b) Lip 25 (radius = 0.00432 c).
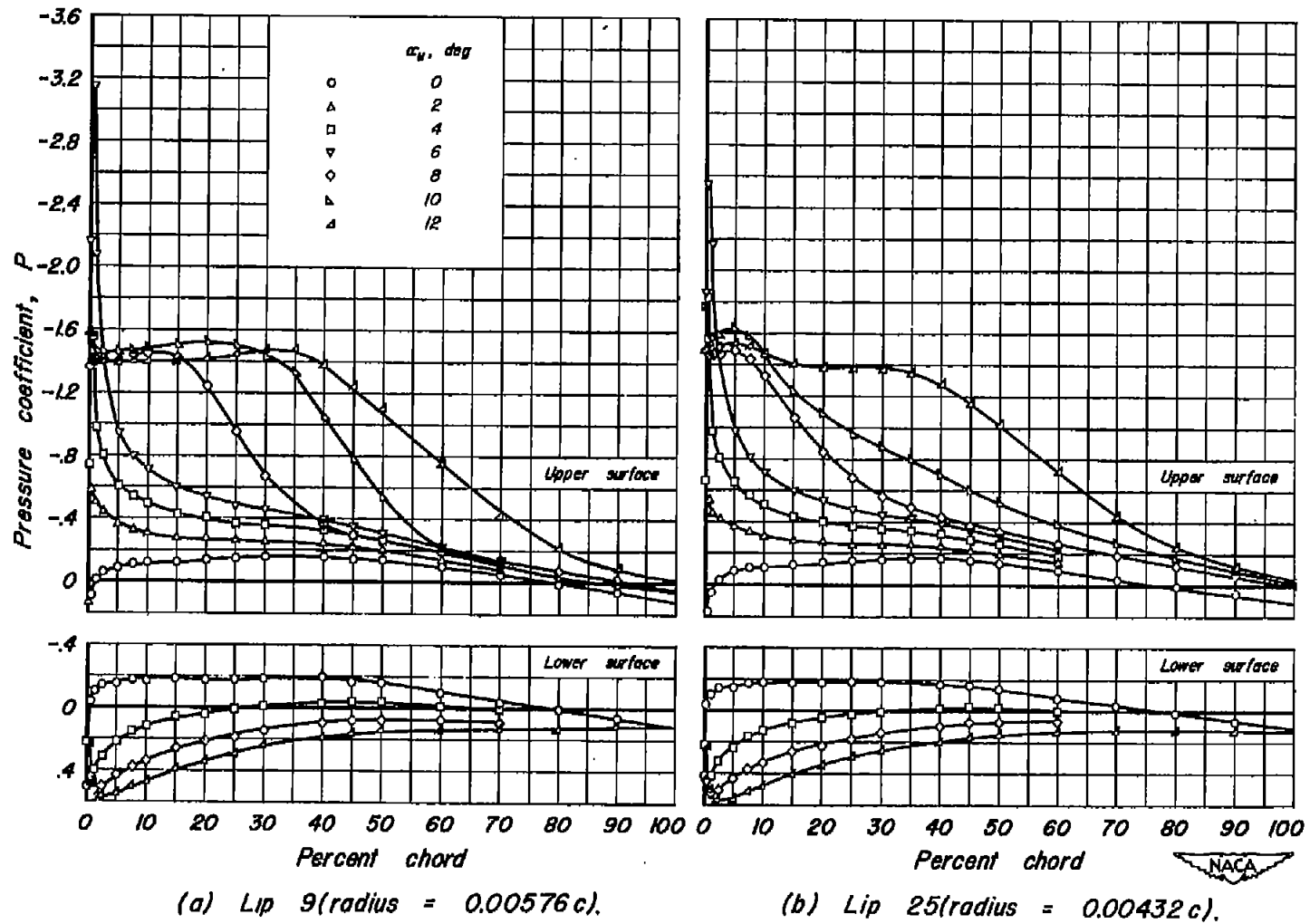
Figure 9.— Chordwise distribution of pressure at the mid span for modifications to the thickness and the lip radius of the upper lip of an inlet having a d/t of 0.20 with 20° stagger. V_1 / V_o, 0.8.
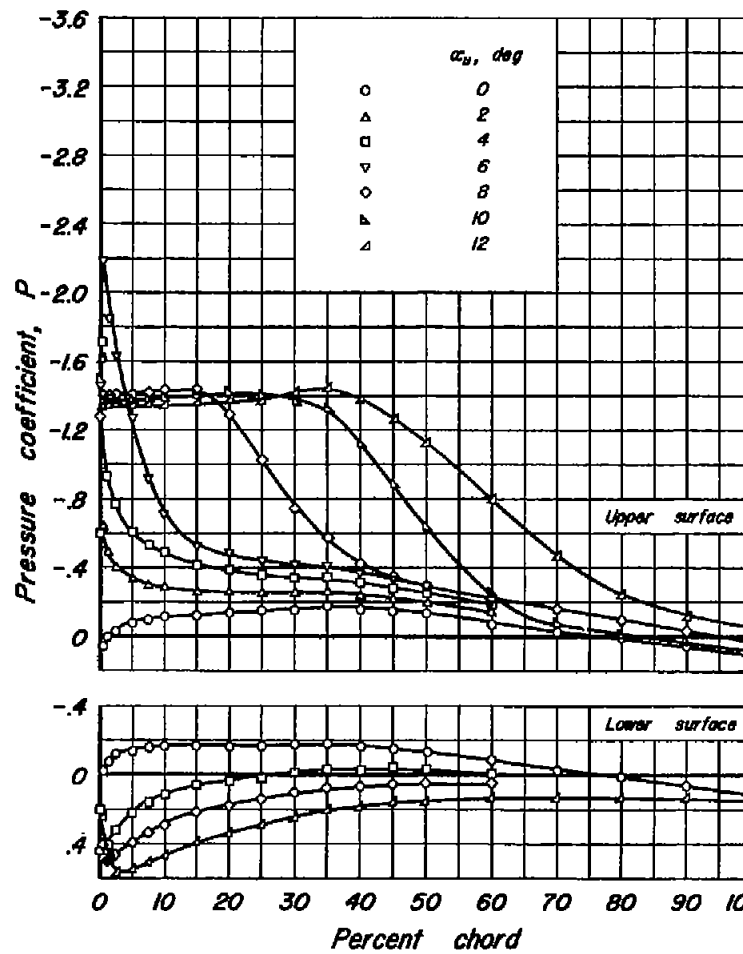
(c) Lip 23 (radius = . 0.00576c).   (d) Lip 21 (radius = 0.00576c).
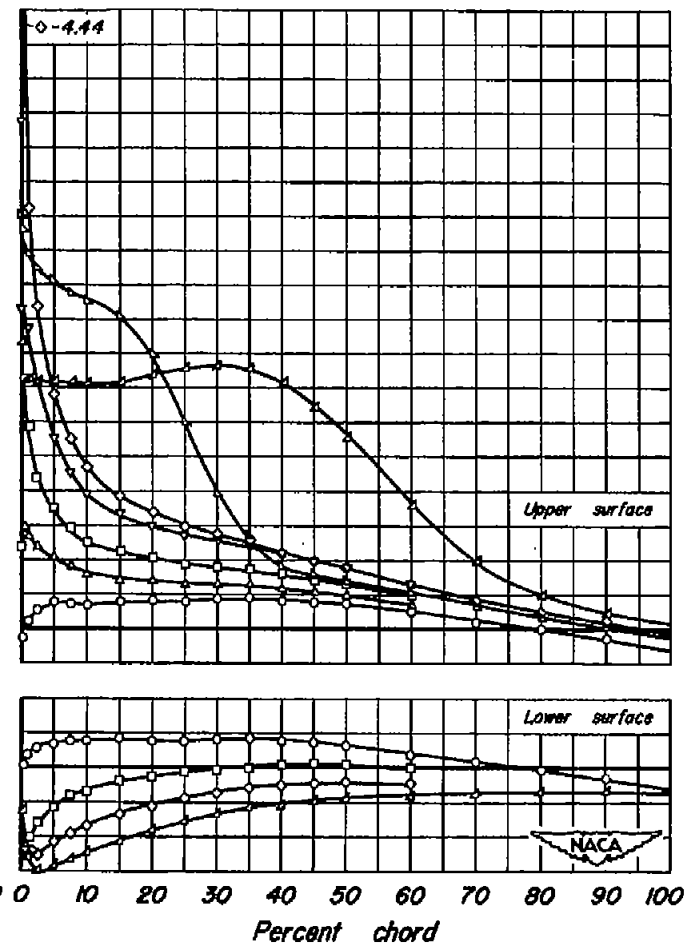
Figure 9.- Concluded.

(a) d/t, 0.15.

(b) d/t, 0.20.

(c) d/t, 0.25.

(d) 20° stagger.
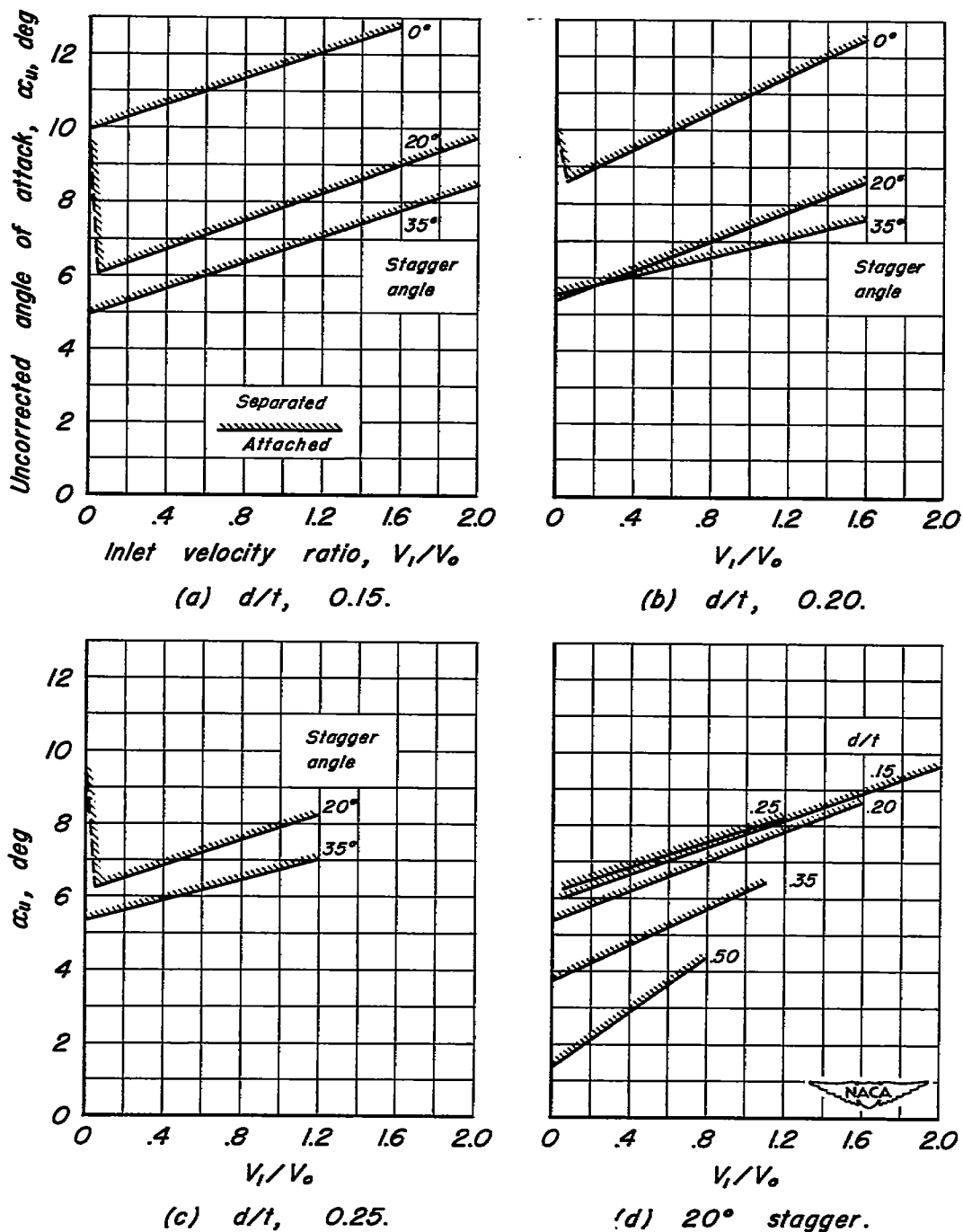
Figure 10.— The variation with inlet-velocity ratio of the angle of attack for flow separation at the midspan for various leading-edge inlets.

(a) Change of leading-edge radius.

(b) Change of thickness distribution.
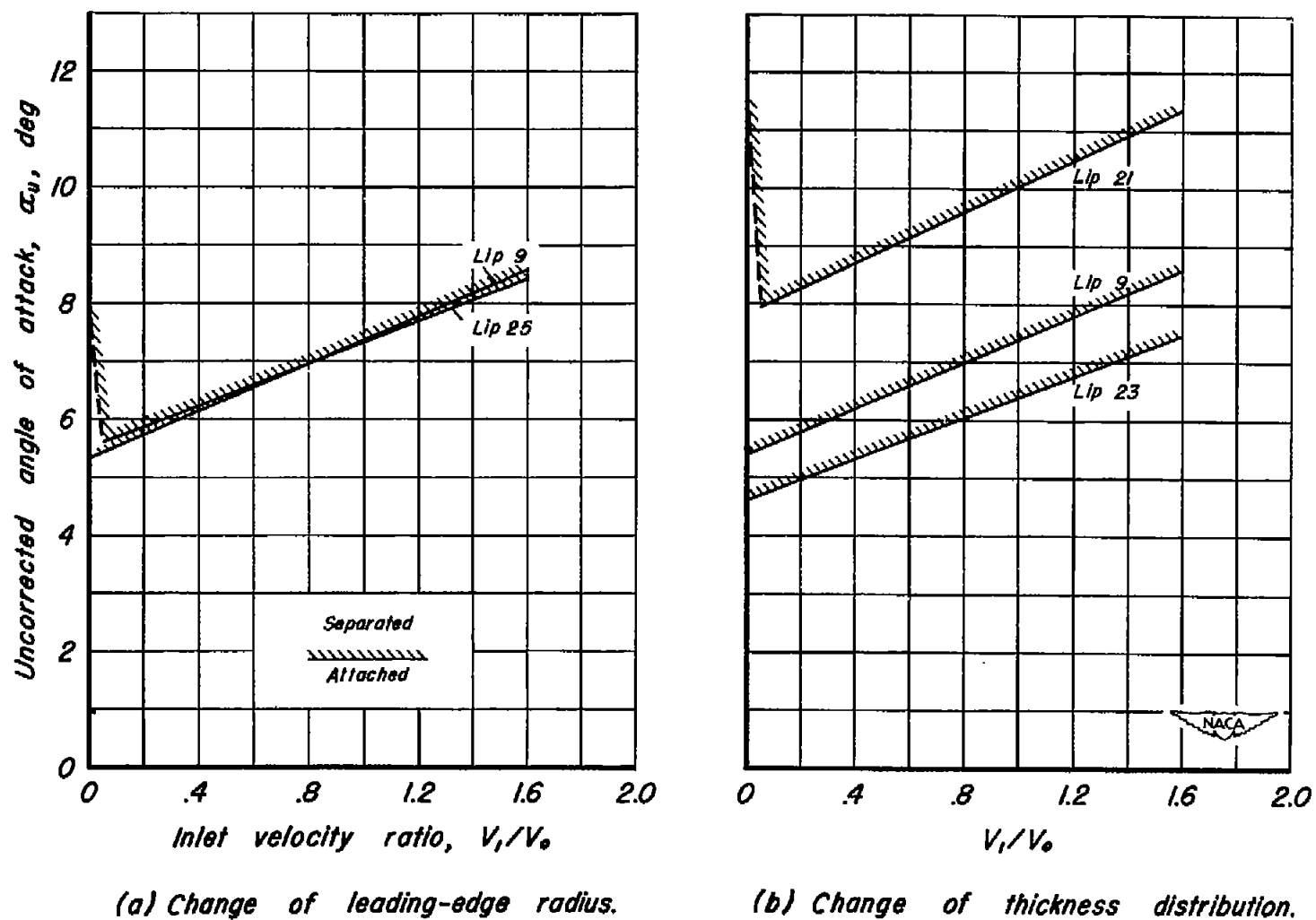
Figure 11.- The effects of changes in leading-edge radius and thickness distribution on the angles of attack for flow separation at the midspan for an inlet having a d/t of 0.20 with 20° stagger.
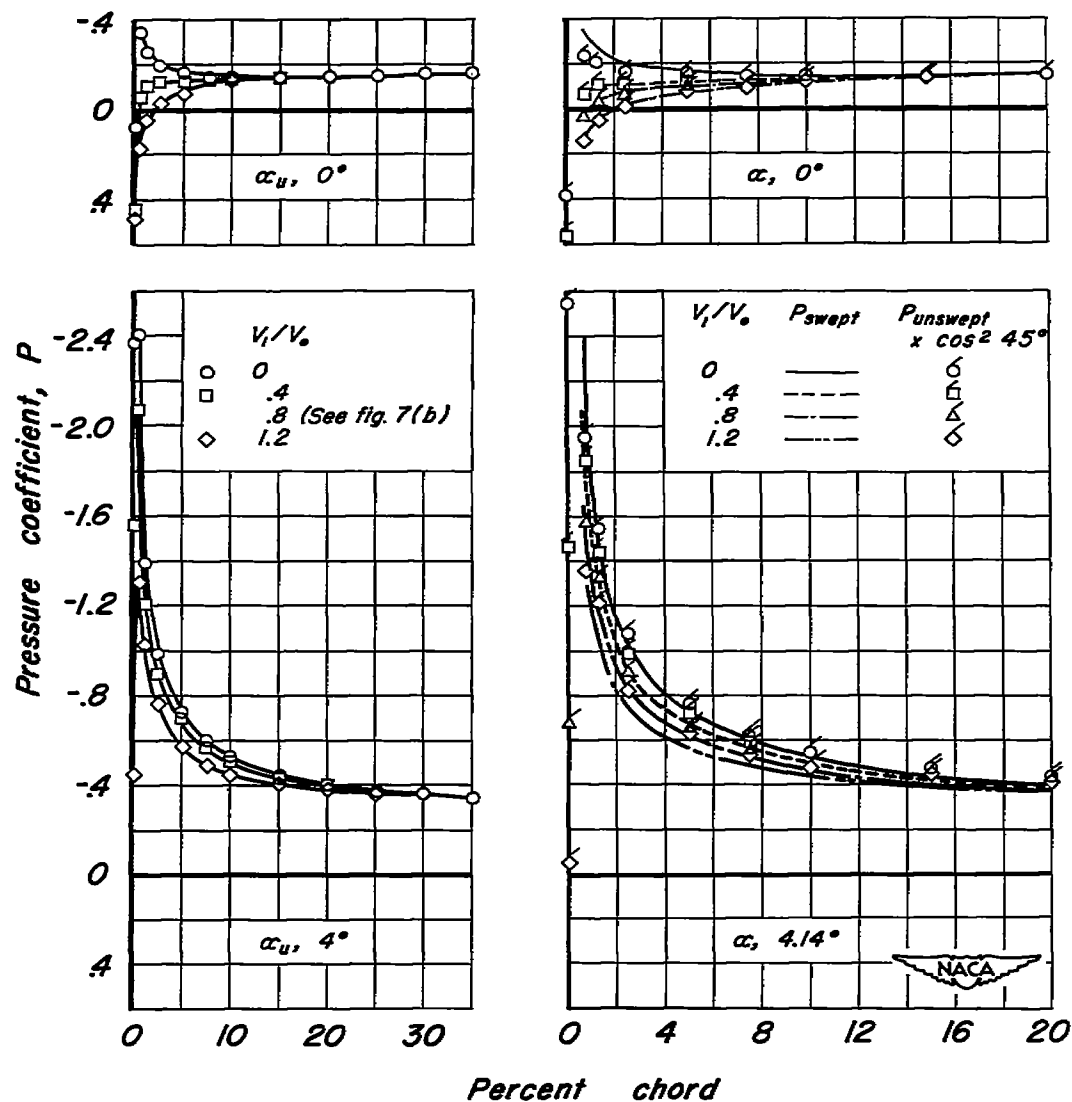
(a) Experiment.   (b) Comparison with predictions.

Figure 12.— Variation of the chordwise distribution of pressure with inlet-velocity ratio at the midspan of inlets having a d/t of 0.25 with 20° stagger.

d/t	φ, deg
0.15	0
.15	20
.15	35
.20	0
.20	20
.20	35
.25	20
.25	35
.35	20
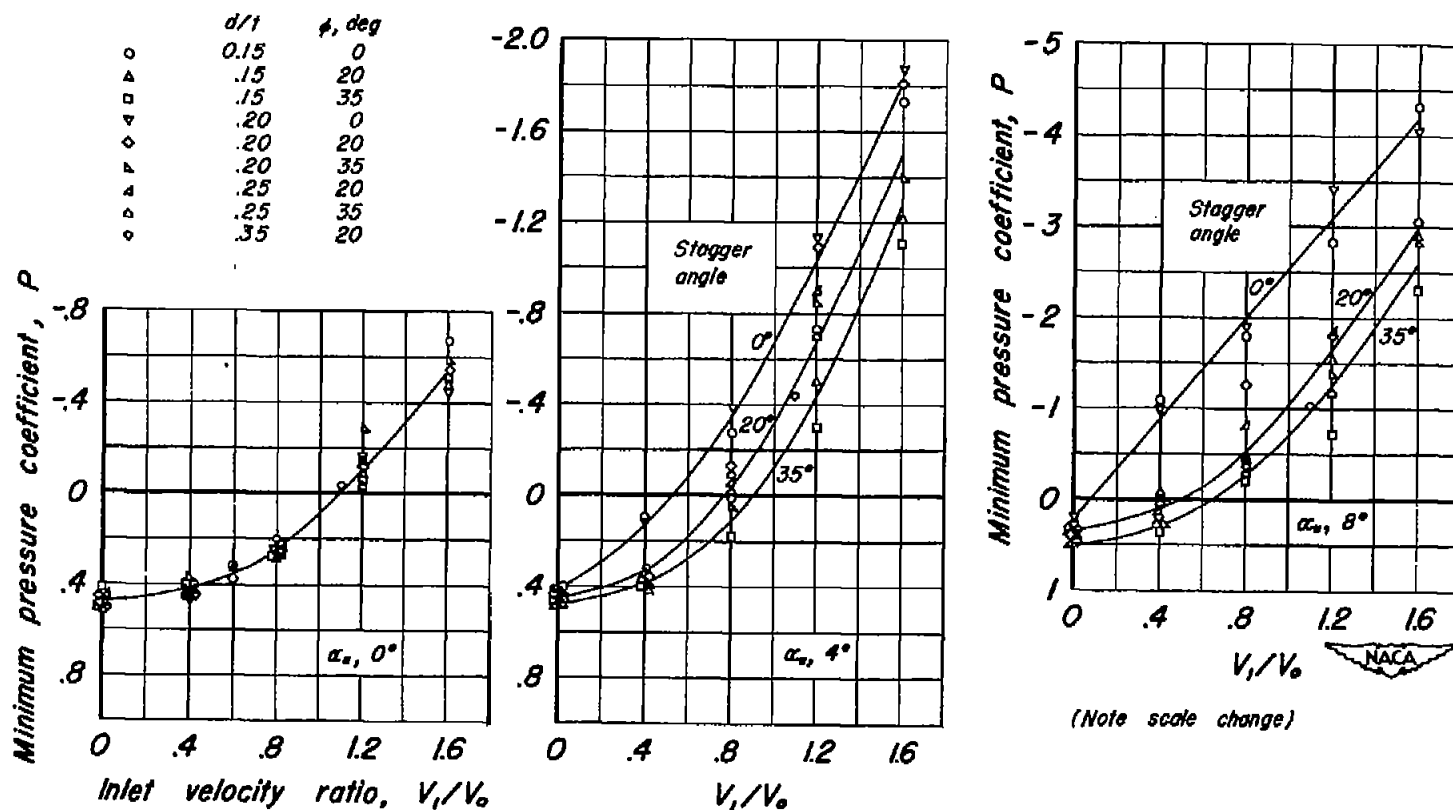
Figure 13.- Effect of inlet-velocity ratio on the minimum pressures on the inside surfaces of the lower lips of various leading-edge inlets.
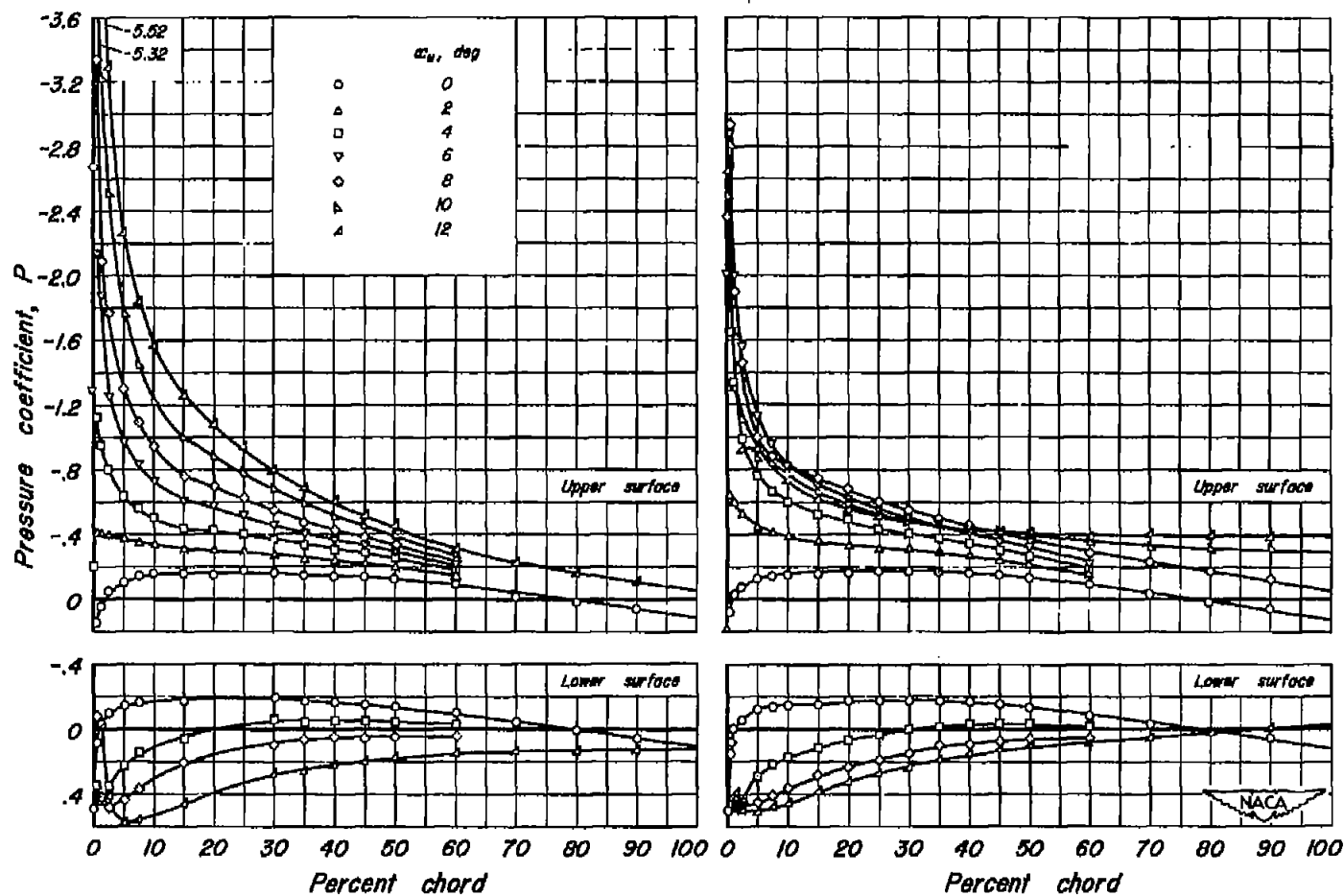
(a) 27.5-percent span station.

(b) 72.5-percent span station.

Figure 14.- Chordwise distribution of pressure at the 27.5- and 72.5-percent span stations for the wing with an inlet having a d/t of 0.25 with 20° stagger. V_i/V_o, 0.8.
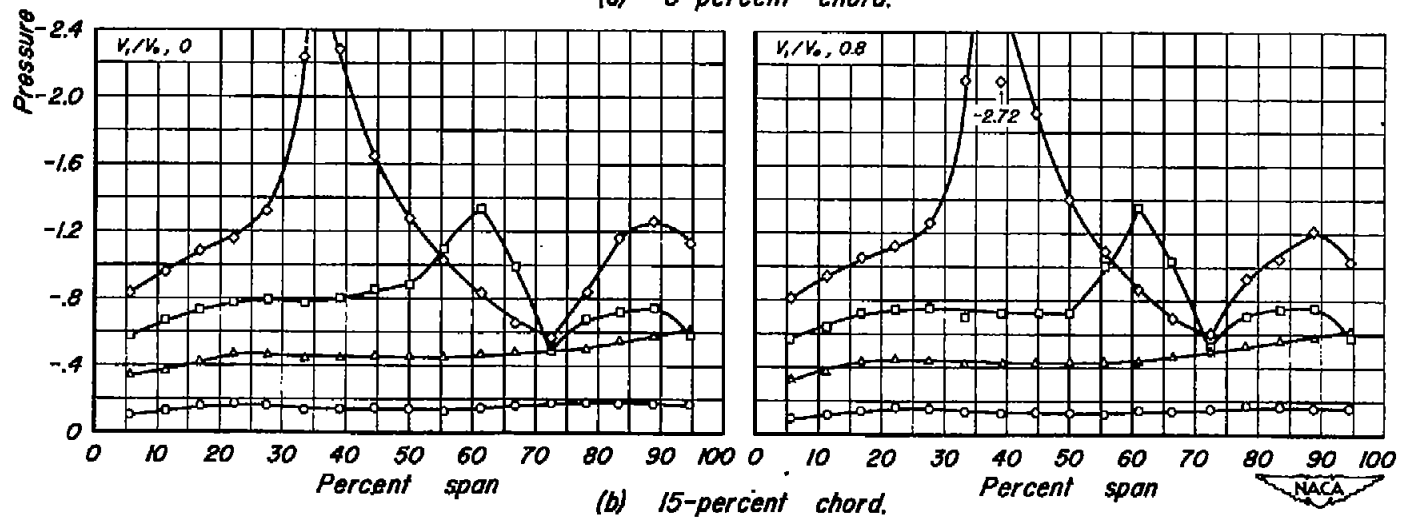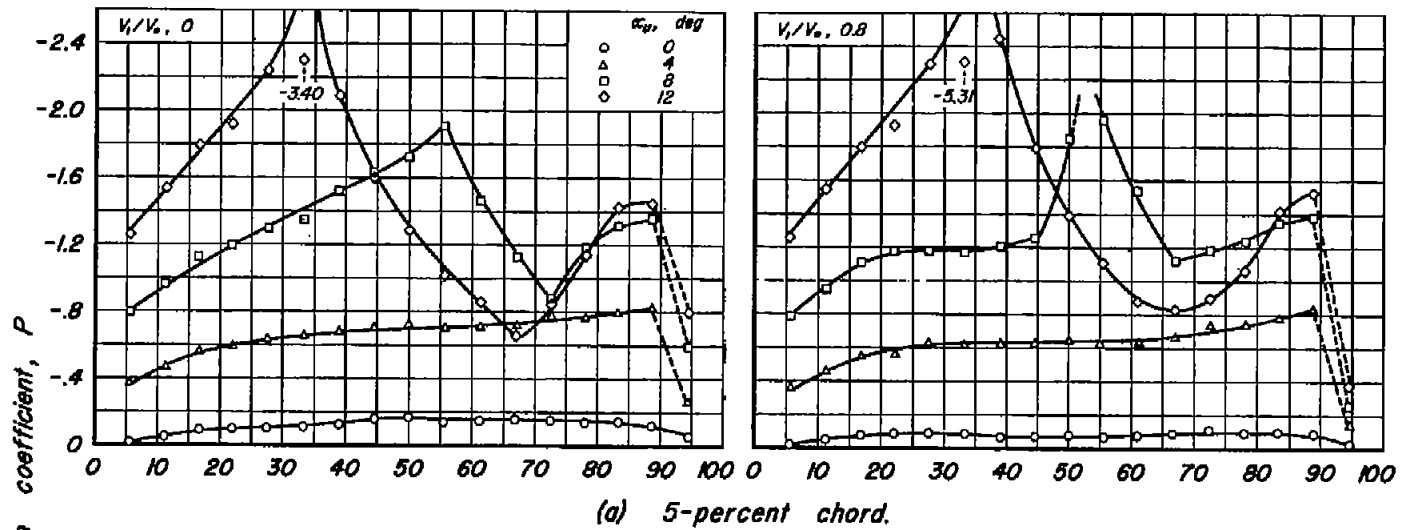
Figure 15.— Spanwise variation of pressure over the upper surface of the wing with an inlet having a d/t of 0.25 with 20° stagger.

(c)   30-percent chord.

(d)   50-percent chord.

(e)   80-percent chord.
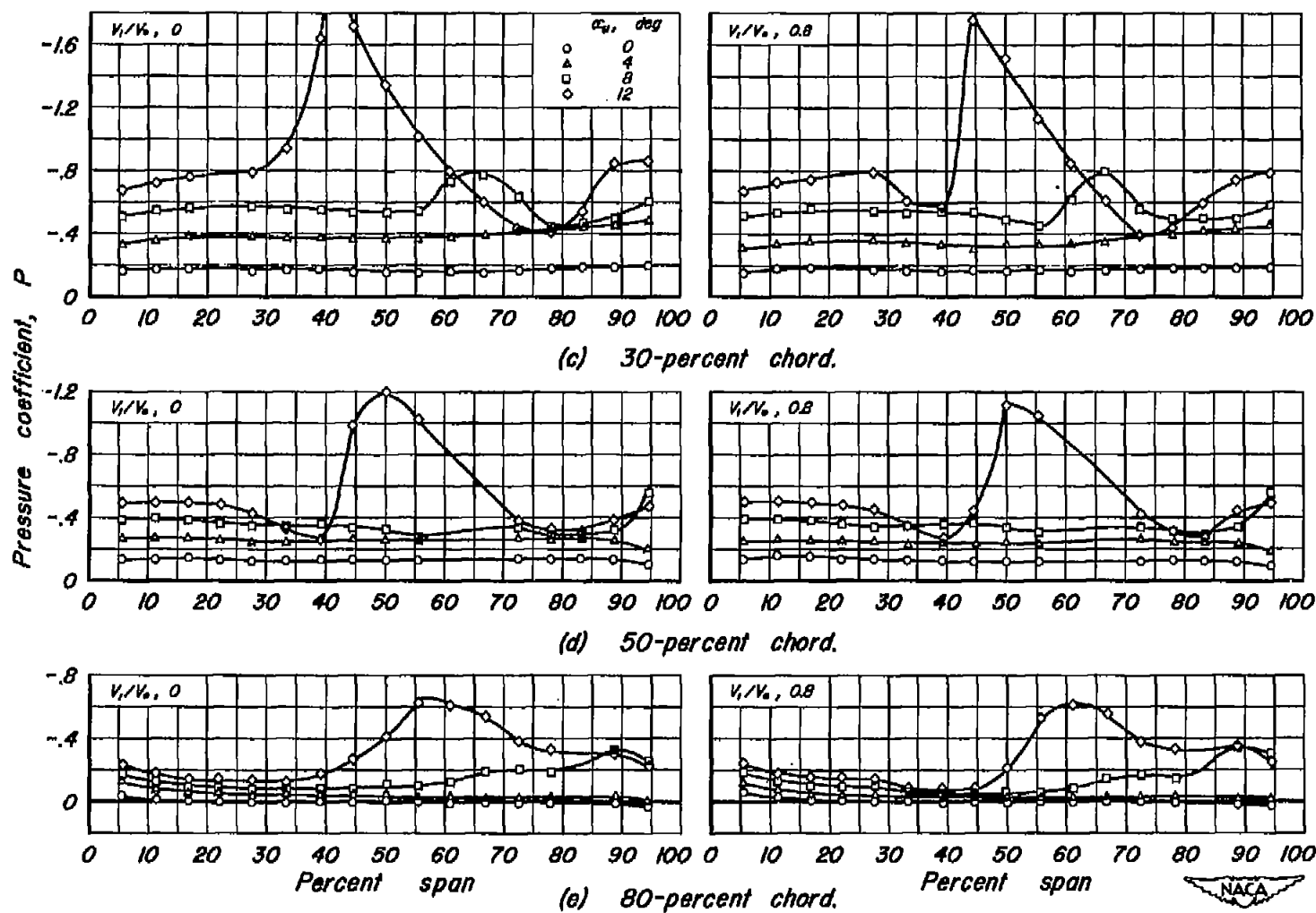
Figure 15.- Concluded.
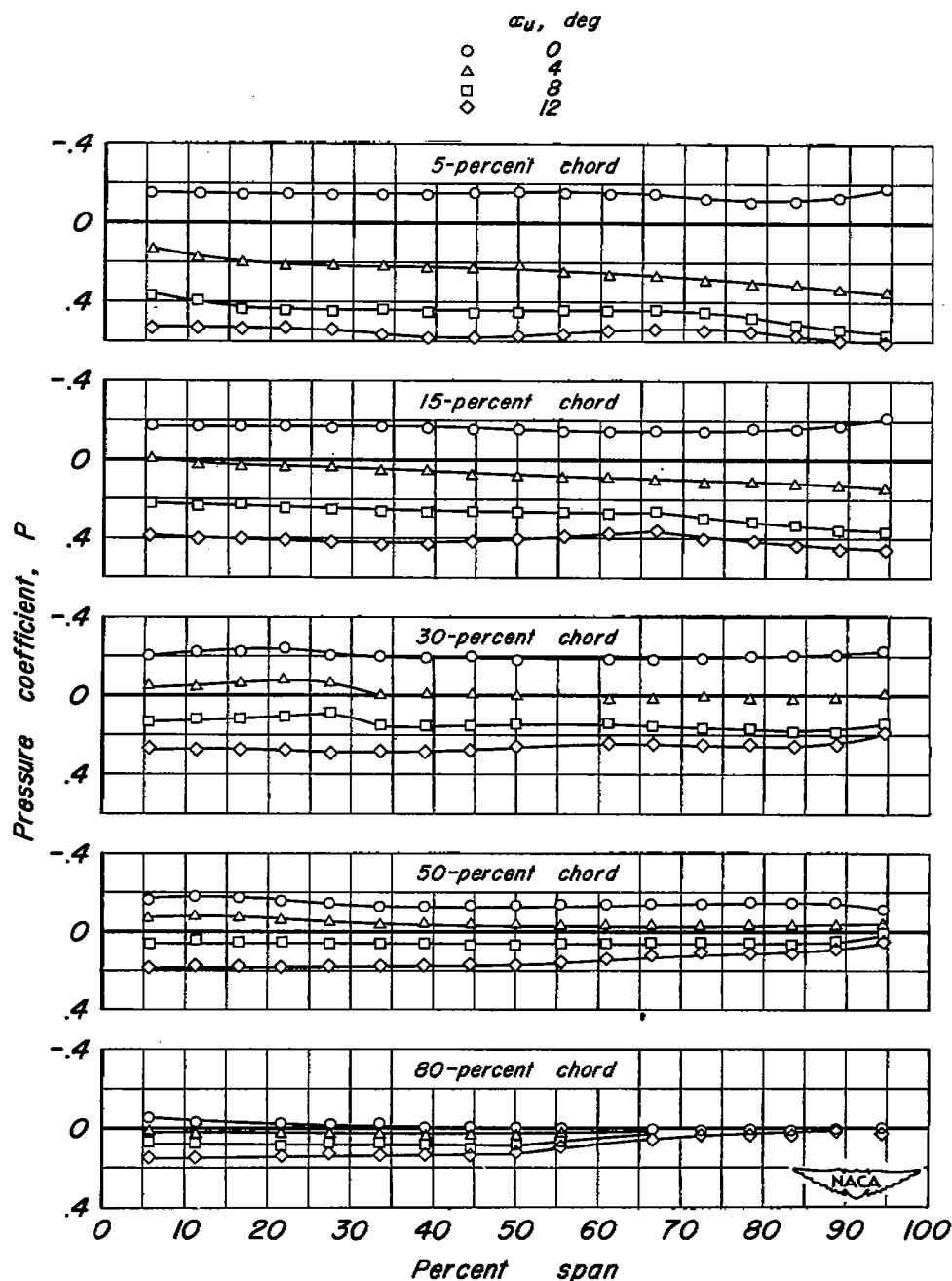
Figure 16.— Spanwise variation of pressure over the lower surface of the wing with an inlet having a d/t of 0.25 with 20° stagger. V_1/V_o, 0.8.
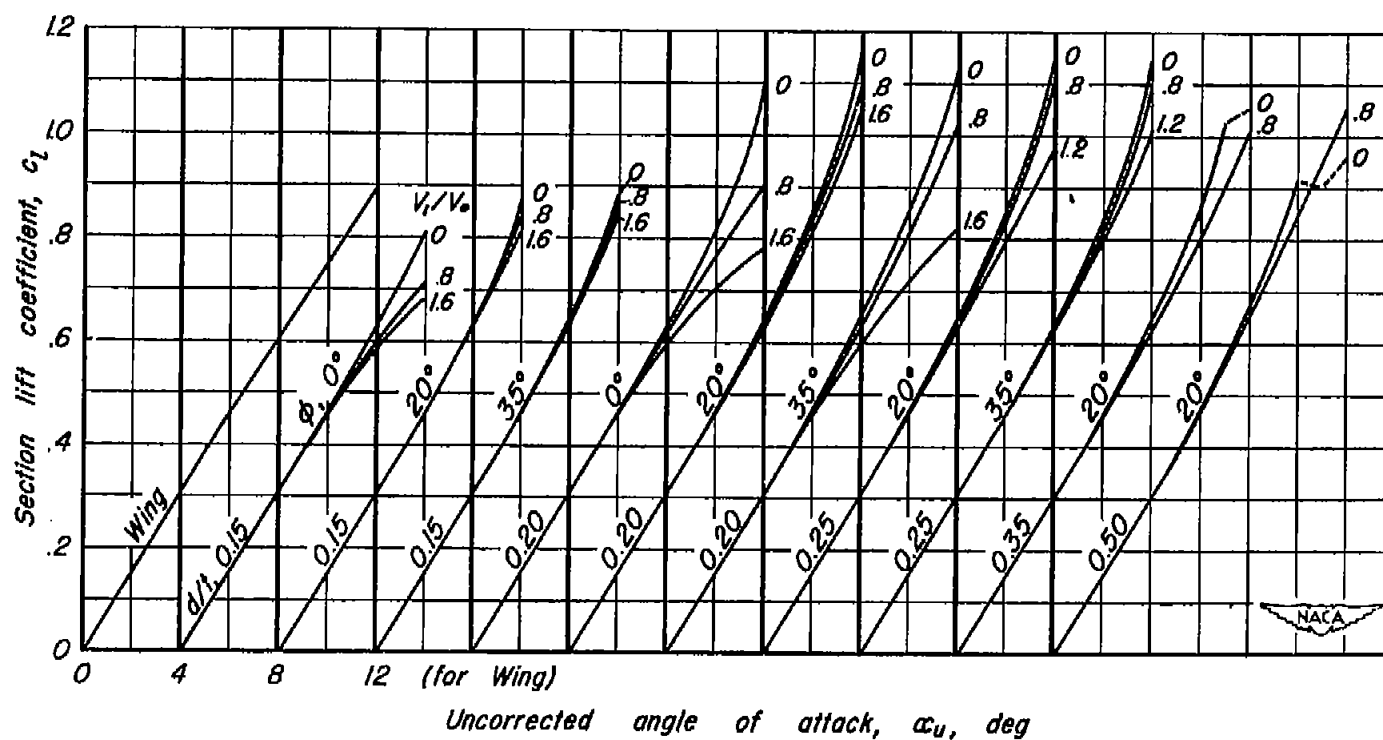
Figure 17.- Section lift characteristics for the midspan of the wing and the wing with various leading-edge inlets.
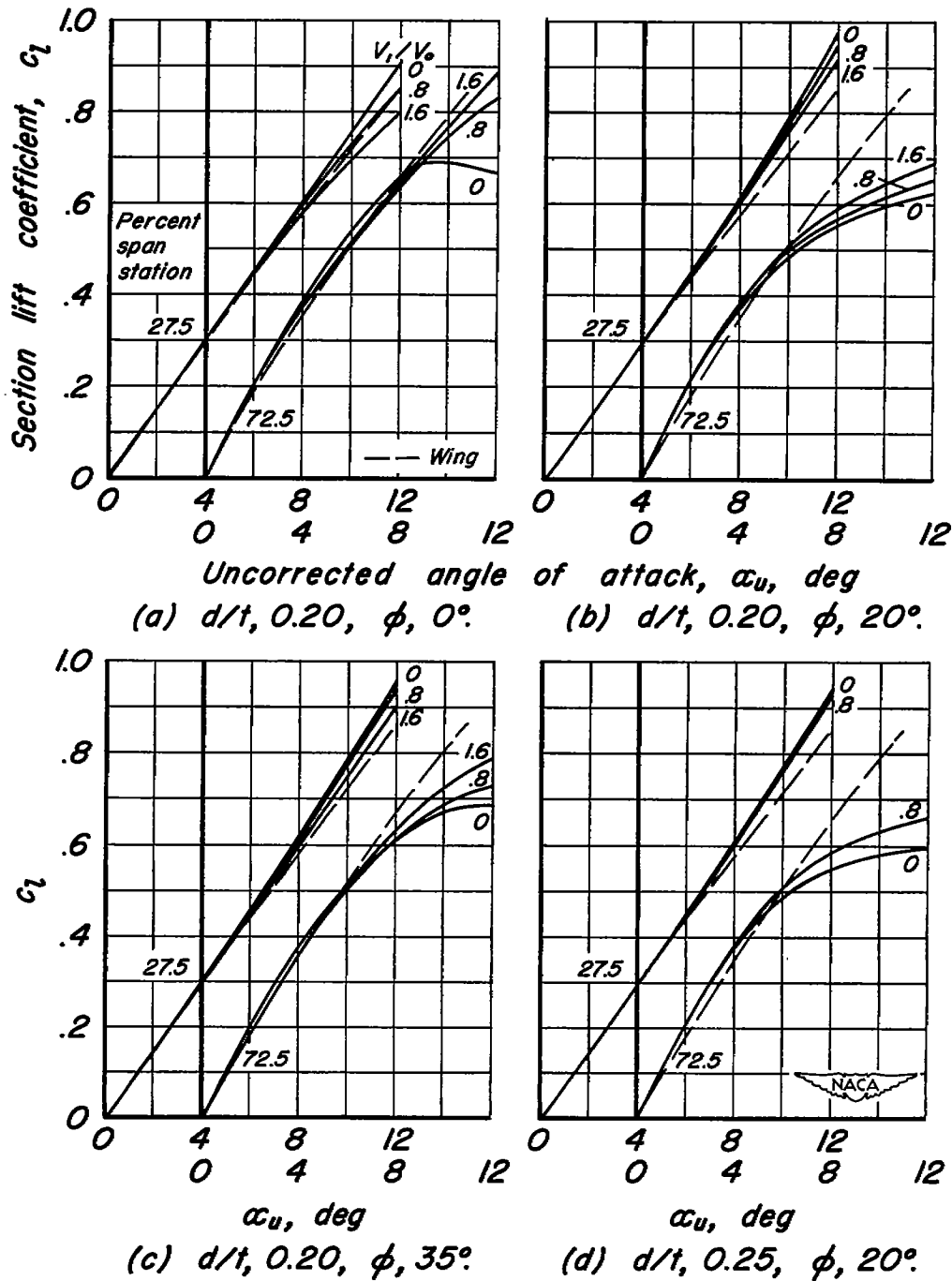
Figure 18.- Lift characteristics of sections at stations 27.5- and 72.5-percent span with various leading-edge inlets.

(a) Midspan station.

(b) 27.5-percent span station.

(c) 72.5-percent span station.
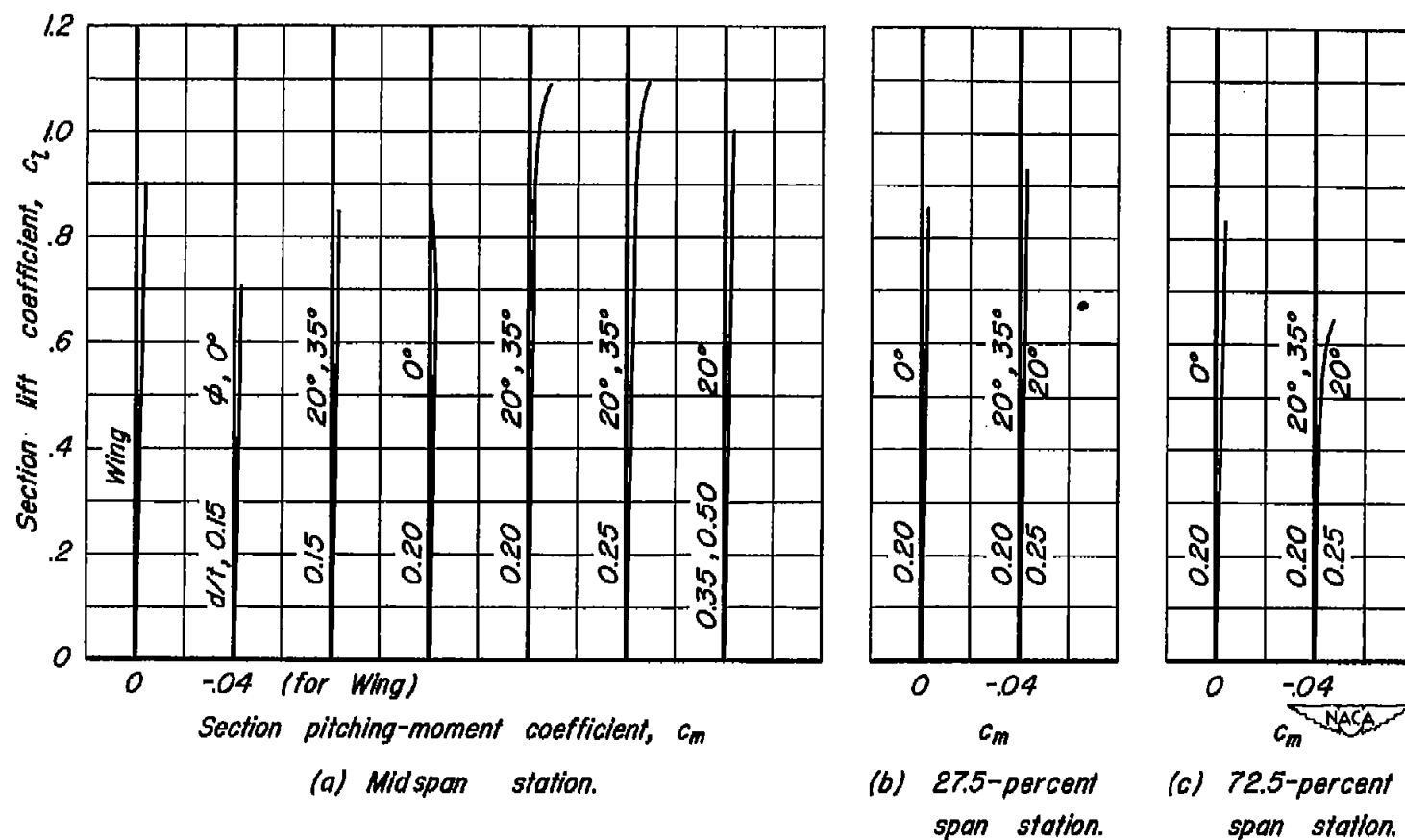
Figure 19.- Moment characteristics for sections of the wing and of the wing with various leading-edge inlets.
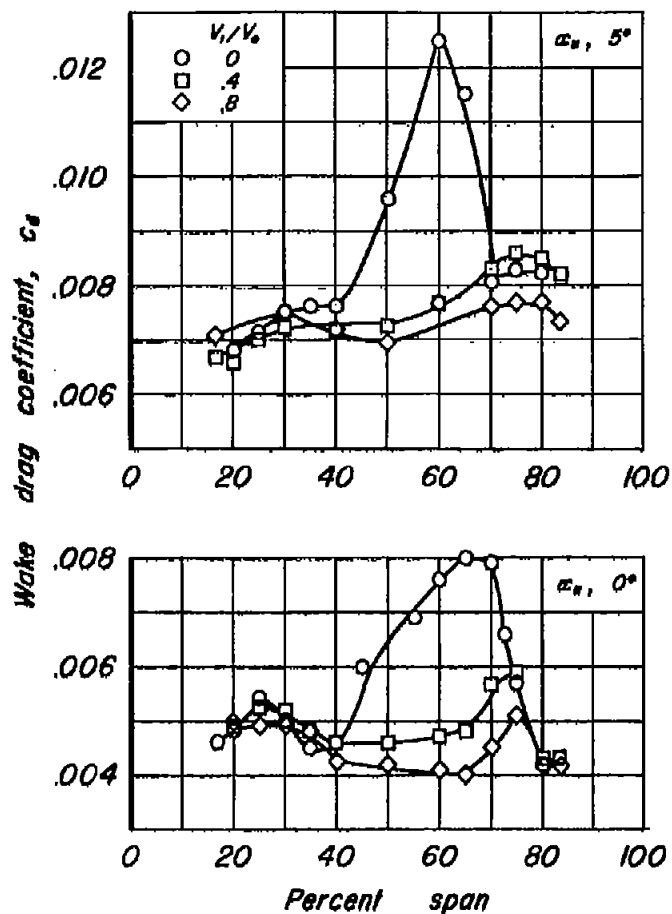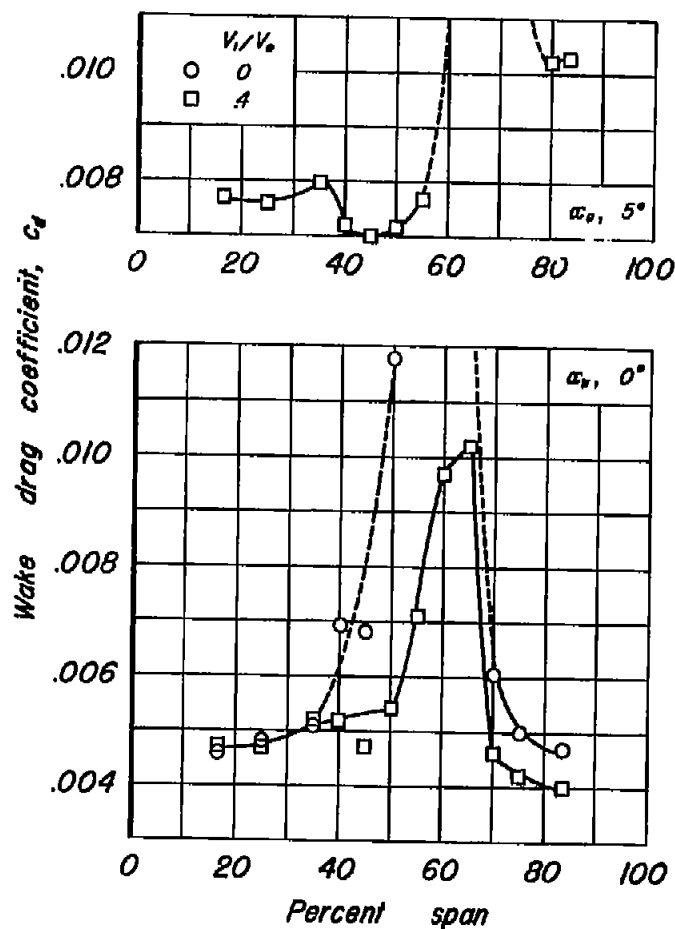
(a) Spanwise variation of wake drag coefficient.
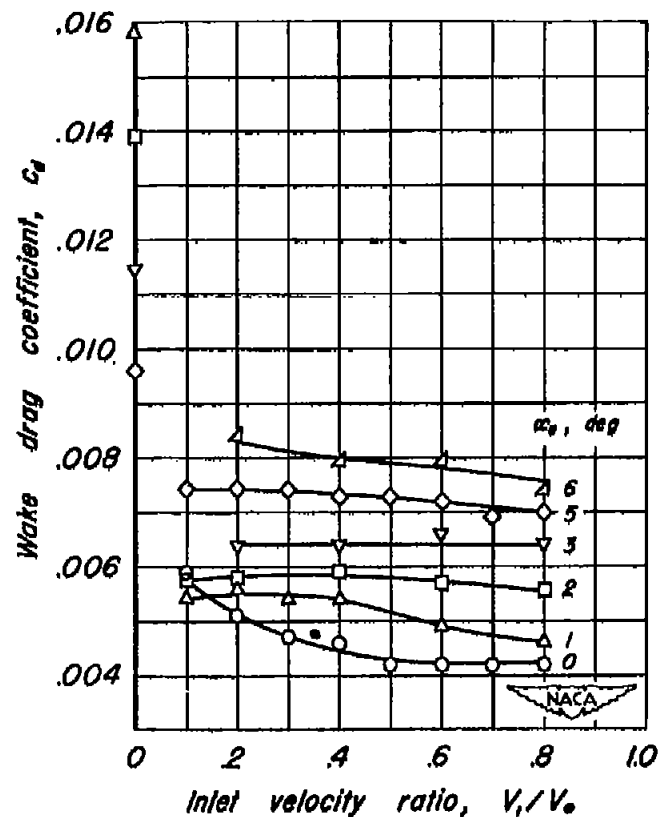
(b) Variation of wake drag coefficient at midspan.

Figure 20.- Wake drag characteristics of the wing with an unstaggered leading-edge inlet having a d/t of 0.20.
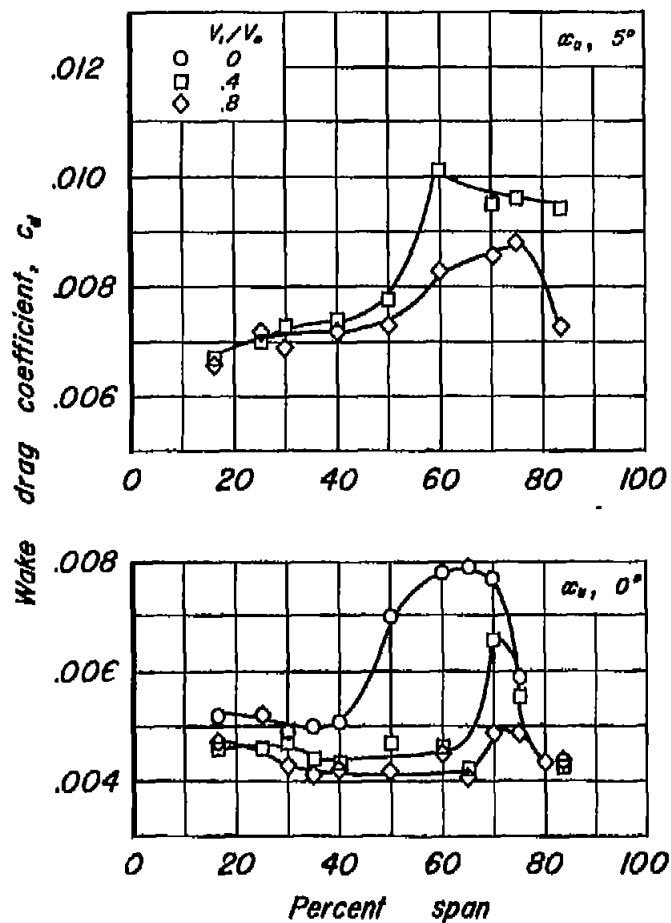
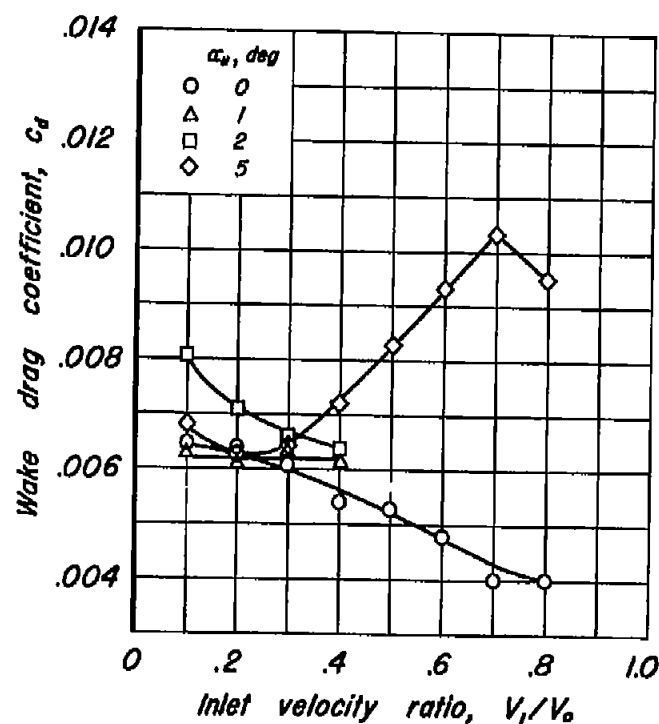(a) Spanwise variation of wake
drag coefficient.
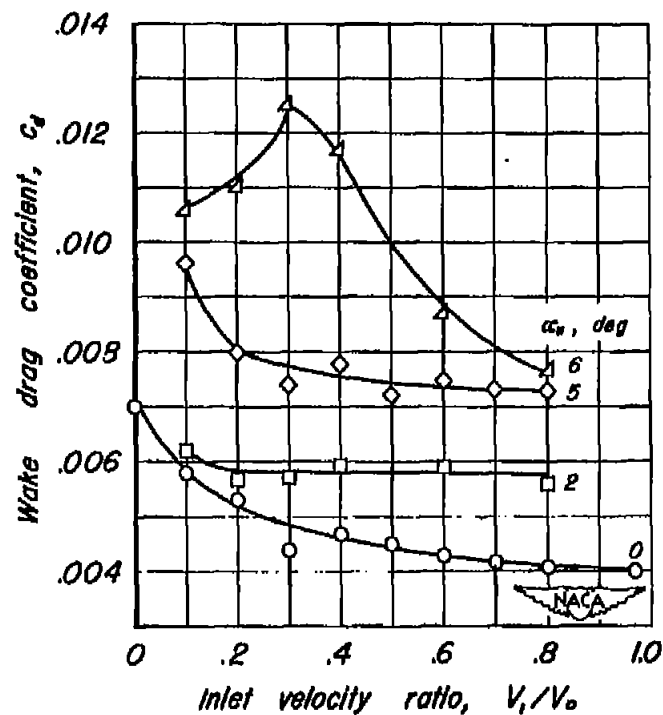
(b) Variation of wake drag
coefficient at midspan.

Figure 21.- Wake drag characteristics of the wing with a leading-edge inlet having a d/t of 0.20
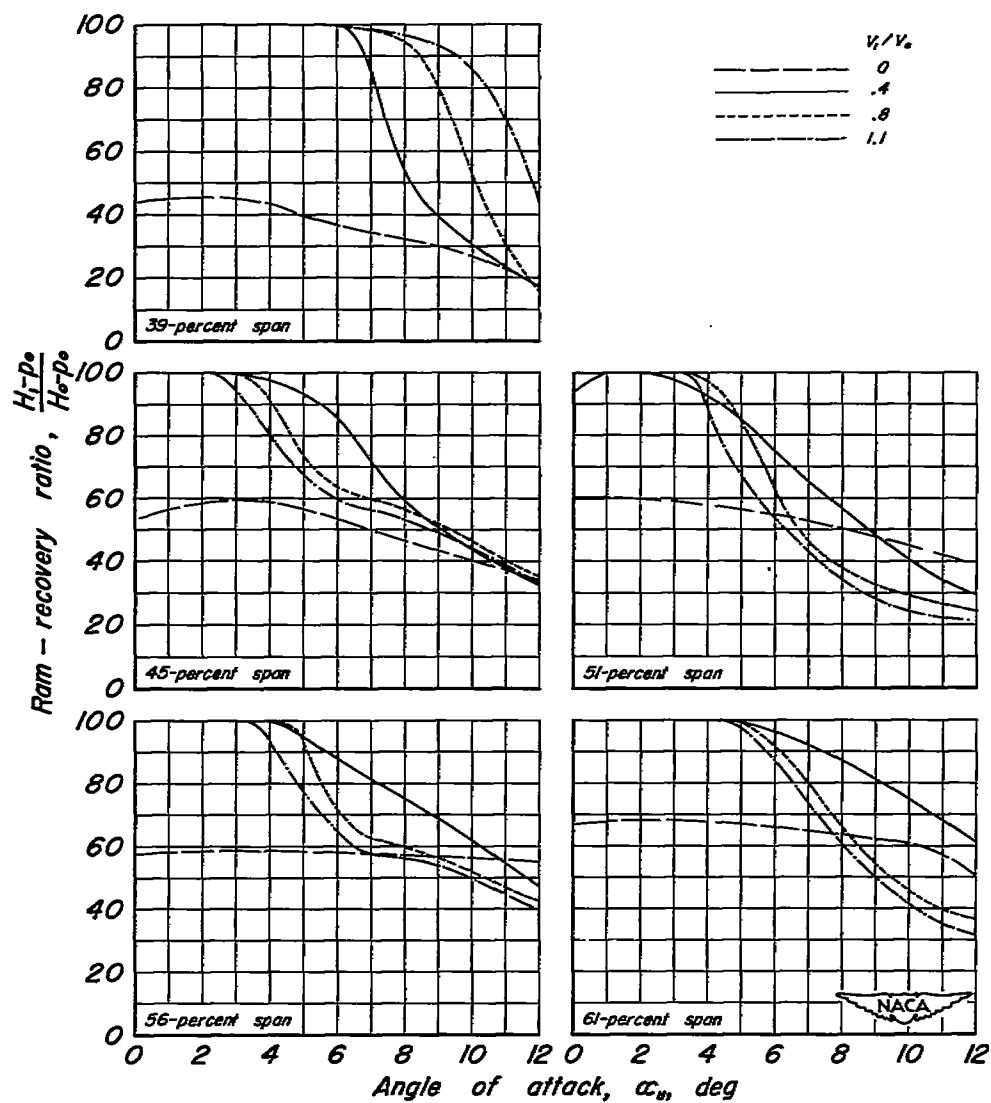with 20° stagger.
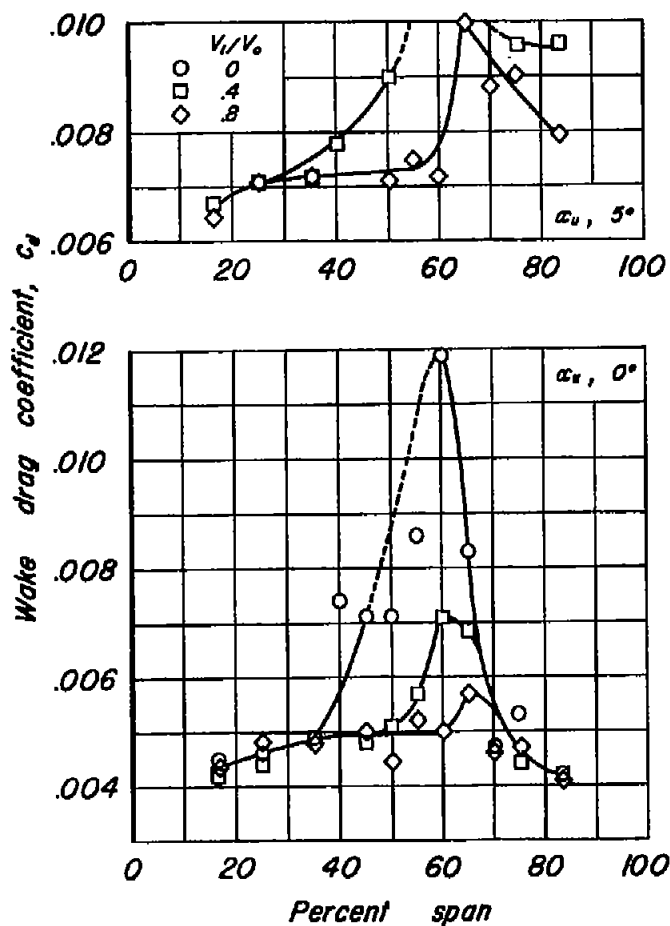
(a) Spanwise variation of wake drag coefficient.
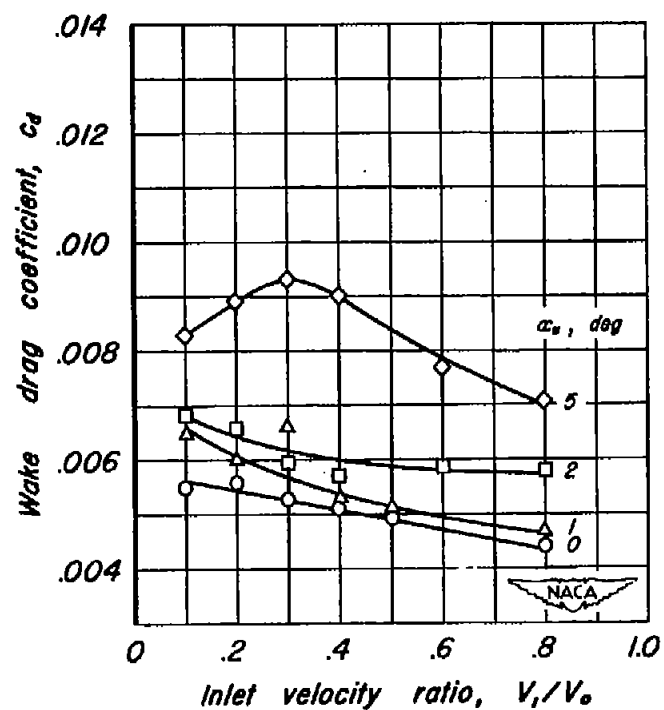
(b) Variation of wake drag coefficient at midspan.

Figure 22.- Wake drag characteristics of the wing with a leading-edge inlet having a d/t of 0.35 with 20° stagger.

(a) Spanwise variation of wake drag coefficient.

(b) Variation of wake drag coefficient at midspan.

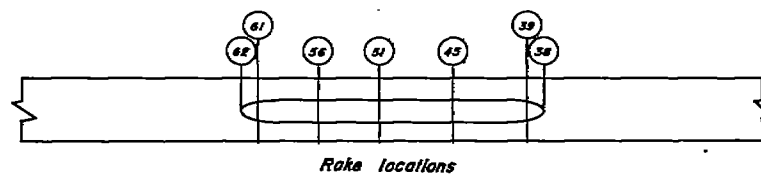Figure 23.- Wake drag characteristics of the wing with a leading-edge inlet having a d/t of 0.50 with 20° stagger.
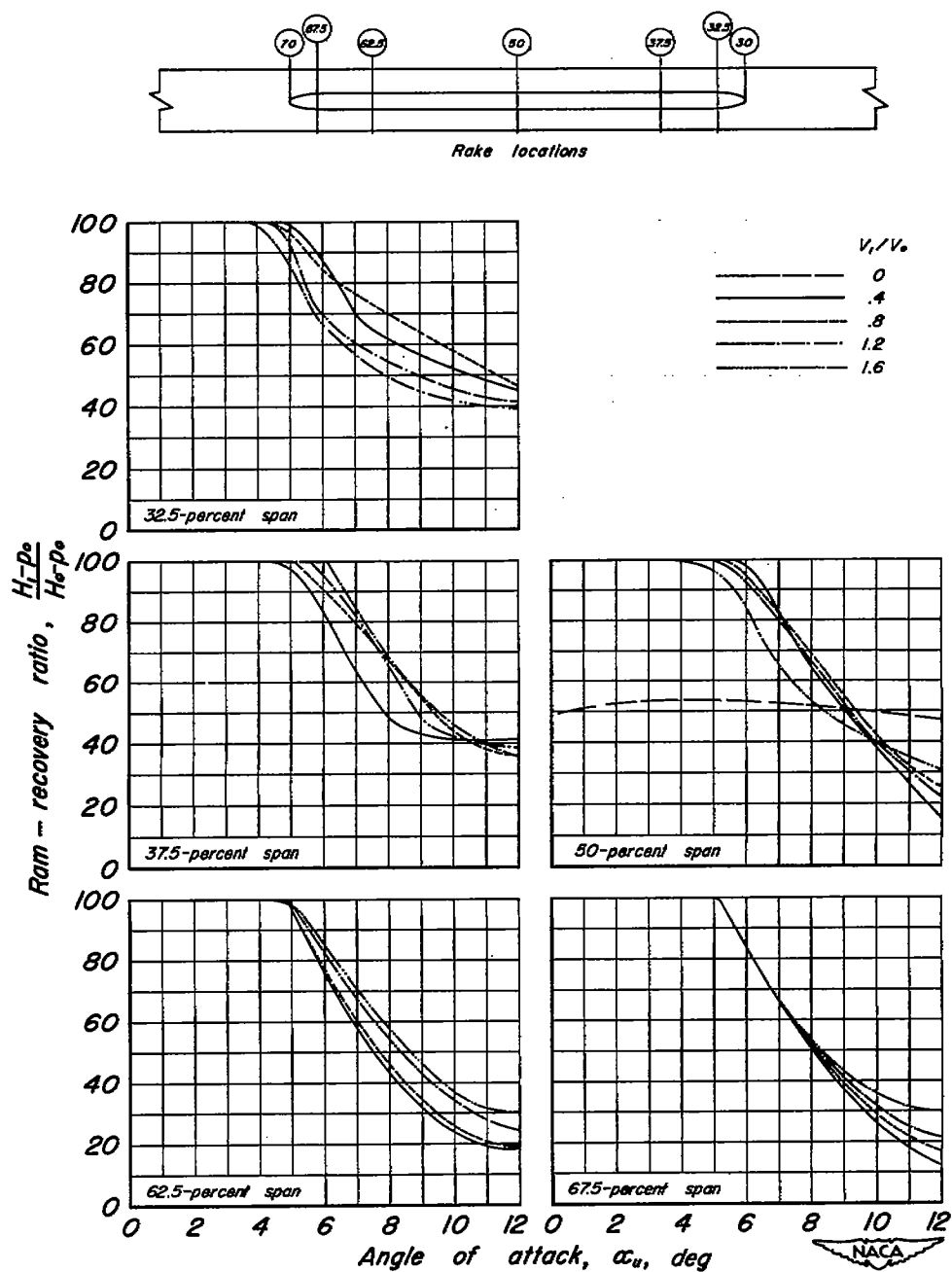
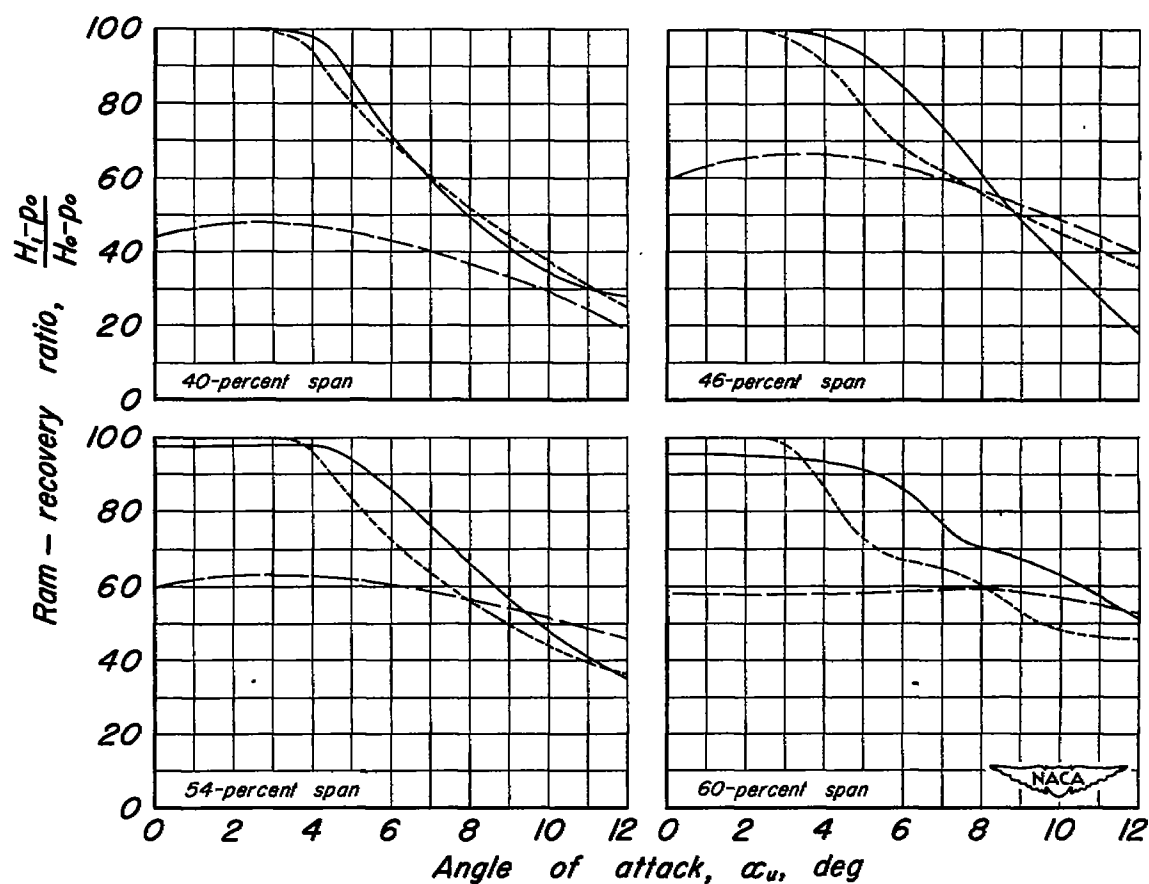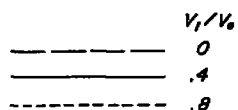(a) d/t, 0.20.

Figure 24.— Ram—recovery characteristics of various leading-edge inlets
with 20° stagger.

Rake locations

V₁/Vₐ
0
.4
.8
1.1

39-percent span

45-percent span

51-percent span

56-percent span

61-percent span

Ram — recovery ratio, $\frac{H_i - p_o}{H_o - p_o}$

Angle of attack, α_s, deg

(b) d/t, 0.35.

Figure 24.— Continued.
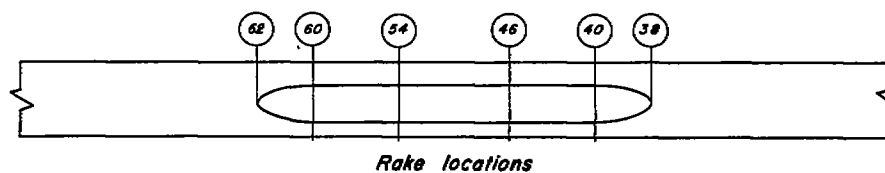
(c) d/t, 0.50.

Figure 24.- Concluded.